An investigation into methods of joining fibre-reinforced plastics for Formula Student

Freddie Bickford Smith, Chris Lo, Alexandros Vossos

Supervisor: Professor Fabrizio Scarpa

April 2017

Abstract

Methods of joining fibre-reinforced plastic components were investigated. Following a literature review, single lap joints between carbon-epoxy laminates were selected as the focus of the project. Three joining methods – adhesive bonding, mechanical fastening and hybrid joining – were considered.

The material properties of the laminates to be joined were studied. Theoretical predictions were variable in their accuracy to experimental results (elastic modulus within 15%; Poisson's ratio within 35%; strength within 55%). Analysis was limited to the in-plane properties of the laminates.

The behaviour of single lap joints was investigated using algebraic solutions, finite element analysis, and mechanical tests. Under tensile loading of the laminates, adhesive bonding was found to produce the strongest and stiffest joints, followed by mechanical fastening. Hybrid joints were the least strong and stiff.

Theoretical analysis proved to be valuable in explaining the underlying mechanics of joint performance. For example, the deformation of joints was demonstrated to have a significant effect on the distribution of stress within them. The accuracy of theoretical models was limited by the validity of the assumptions on which they were based. Allman's two-dimensional analysis of adhesive joints produced predictions within 25% of average testing results. Estimations based on an assumption of material isotropy predicted the failure load of mechanically fastened joints within 10% of experimental findings. More work is required to develop an accurate theoretical model of hybrid joints, which failed at lower loads than expected.

Work allocation

Allocation of report writing is denoted by author initials in section headings, where FBS corresponds to Freddie Bickford Smith, CL corresponds to Chris Lo, and AV corresponds to Alexandros Vossos. The table below shows work allocation throughout the project.

Task	Freddie	Chris	Alex
Literature review	X	X	X
Adhesive selection	X	X	X
Theoretical analysis of laminates	X	X	
Theoretical analysis of adhesive bonding	X		
Theoretical analysis of mechanical fastening			X
Theoretical analysis of hybrid joining	X		X
Manufacturing		X	X
Testing	X	X	X
Report writing	X	X	X
Report editing	X		

I hereby confirm that the table above provides an accurate and fair representation of the allocation of work between project group members.

Title	An investigation into methods of joining fibre-reinforced plastics for Formula Student		
Signatures			
Authors	Freddie Bickford Smith	Chris Lo	Alexandros Vossos
Date	24 April 2017		

Figures

Tables

Contents

1 Introduction [FBS]

The requirement to assemble structures with fibre-reinforced plastic components necessitates a clear guide on how join them. The aim of this project was to investigate methods of joining fibre-reinforced plastics in the context of Formula Student, a university motorsport competition. This was achieved by completing three primary objectives:

1. Review literature on fibre-reinforced plastics and joining methods to identify subject areas to investigate
2. Characterise the chosen materials and joining methods
3. Use findings to develop a high-level guide to the analysis and design of joints between fibre-reinforced plastics

1.1 Fibre-reinforced plastics [FBS]

Fibre-reinforced plastics are composite materials made of two components – high strength and stiffness fibres, and a polymer matrix – with distinct interfaces between them [1]. The fibres provide the principal load-carrying capacity. The surrounding matrix maintains fibre position and orientation, transfers loads between fibres, and protects fibres from environmental damage. The combination of materials results in different properties to those of the individual components. Commonly used fibres include carbon, glass, and aramid. They can be of continuous or discontinuous length, and of controlled or random orientation. The matrix can be either a thermosetting polymer (such as epoxy, phenolic or bismaleimide) or a thermoplastic polymer (such as PEEK) [2].

Fibre-reinforced plastics are widely used in high-performance automotive applications [3], with examples shown in Figure 1. In this context, carbon-epoxy composites (continuous carbon fibres embedded in epoxy resin) are particularly popular [4]. The widespread use of this fibre-reinforced plastic can be attributed, in part, to its high specific strength (strength/density) and specific stiffness (modulus/density). Compared with a typical aerospace aluminium alloy, unidirectional carbon-epoxy composite has approximately 9 times greater specific strength, and 3 times greater specific stiffness. It offers additional advantages: it provides excellent resistance to corrosion and fatigue; its low coefficient of thermal expansion leads to dimensional stability over wide temperature ranges; and, with high internal damping, it reduces the amplitude of vibrations transmitted through structures [1, 2].

In structural applications, fibre-reinforced plastic is most commonly used in the form of a laminate, which is made by stacking multiple thin layers of reinforcement (also known as ‘laminae’ or ‘plies’), infusing them with the matrix, and consolidating the stack into the desired thickness [1]. Rolls of continuous fibre come either in unidirectional or woven form, as shown in Figure 2. In unidirectional reinforcement, all fibres are straight and parallel. Woven reinforcement is made by passing fibres in the ‘weft’ direction alternately

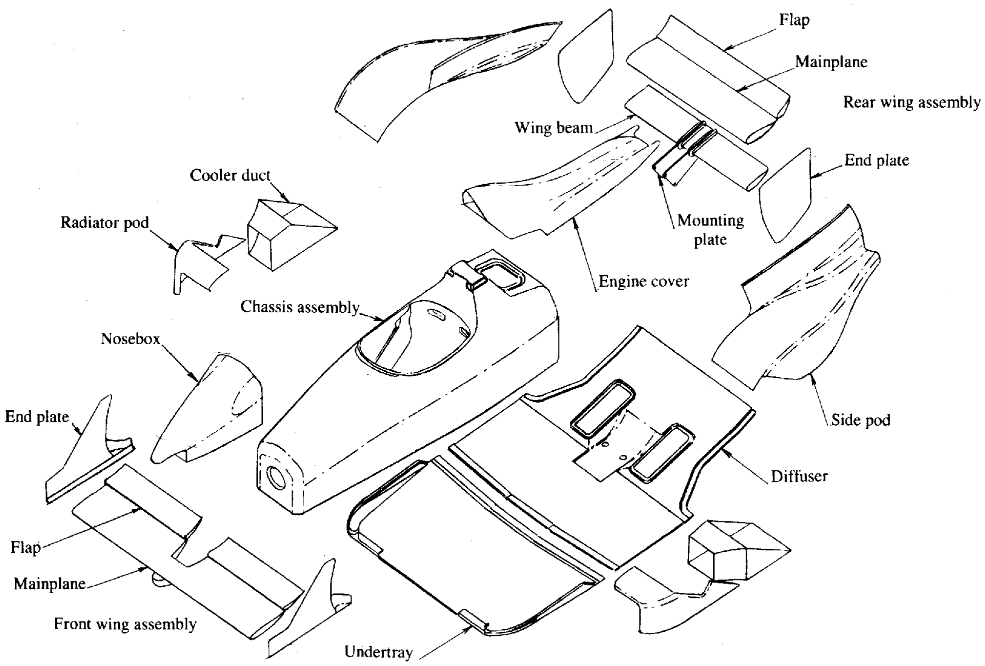

Figure 1: Racing car components made of fibre-reinforced plastic (from [3])

under and over fibres in the 'warp' direction, resulting in fabric with equal proportions of fibres oriented in each direction. The woven architecture results in 'crimping' (bending) of the fibres, which reduces their load-carrying capacity [1]. However, the flexibility of this fabric facilitates its use in parts with complex curvature [5]. Non-crimp multidirectional fabrics, which are produced by stitching together stacked sheets of unidirectional fibres, can alternatively be used [6].

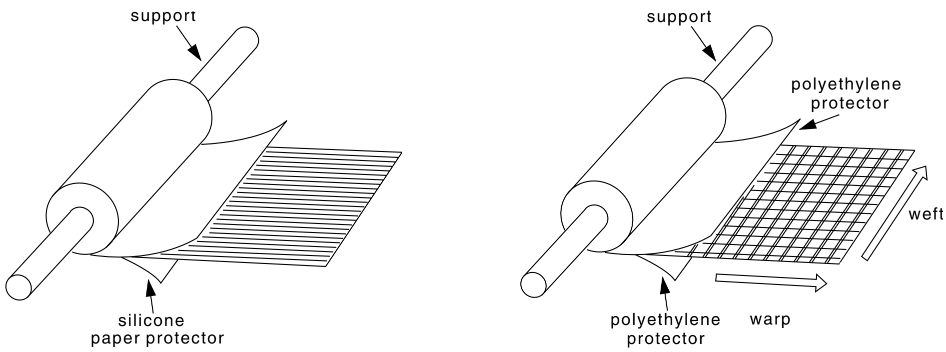

(a) Unidirectional (b) Woven

Figure 2: Different forms of continuous fibre reinforcement (from [7])

Due to their construction, continuous fibre laminates are anisotropic. This means that their materials properties are not the same in all directions [1]. The most extreme case of this is in laminates with unidirectional stacking sequences (or 'lay-ups'), where every layer of fibre reinforcement has the same orientation (see Figure 3a). This produces a material that is considerably stronger in the longitudinal (fibre) direction than in any other.

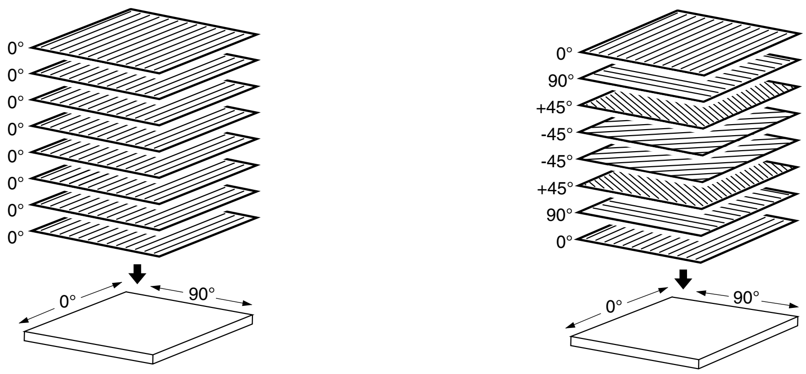

(a) Unidirectional (b) Quasi-isotropic

Figure 3: Variations of stacking sequence in laminates (from [7])

A lay-up in which plies are stacked at angles to each other reduces the significance of anisotropy. Indeed, laminates with certain lay-ups, such as that shown in Figure 3b, are termed 'quasi-isotropic' because their in-plane mechanical properties vary less with orientation when compared to unidirectional laminates. Thus, fibre-reinforced plastics provide an opportunity to tailor the material properties to the design requirements, but they also present analytical challenges not encountered with traditional structural metals [1]. In this project, work was focussed on carbon-epoxy laminates with quasi-isotropic lay-ups. The Formula Student team at the University of Bristol currently uses this type of fibre-reinforced plastic in its car, and plans to use it as the principal material in future versions of the chassis [8].

1.2 Formula Student [FBS]

Formula Student is an annual motorsport competition run by the Institution of Mechanical Engineers for university undergraduates. Teams design and build single-seat, open-wheel racing cars, which are assessed for their design merits as well as on-track performance [9]. In this context, designers must consider not only performance-related objectives, such as straight-line acceleration and speed of cornering, but also matters of practicality and economics. Much of the manufacture and assembly of the car is performed manually, so robustness is essential in design. Cost efficiency is similarly important due to budget constraints. The requirements and capabilities of the Formula Student team inform the set of design criteria presented in Section 6.3. They also serve to limit the overall scope of this project: analysis was conducted to a level of detail judged to be useful to the student designer.

1.3 Joining [FBS]

Load-carrying joints are often unavoidable in physically large structures: manufacturing processes impose limits on the maximum size of a component. Joints might also be desirable: inspection, repair and transportation can be made easier by using assemblies rather than single parts [10].

Swift and Booker [11] identified four categories of joining methods – welding, soldering and brazing, adhesive bonding, and mechanical fastening. Additional techniques exist. Multiple fibre-reinforced plastic parts can be integrated into one by co-curing, where components are assembled into the desired configuration before the curing process (where the matrix 'sets', becoming rigid) is initiated [2, 14]. Alternatively, mechanical fastening elements can be either co-cured into or bonded onto structures, giving hybrid joining methods [13].

This project was focussed on methods of joining composite laminates with thermosetting matrices that have already been cured, thus limiting the set of applicable joining methods to three – adhesive bonding, mechanical fastening, and hybrids of the two [10, 12, 13]. These are illustrated schematically in Figure 4.

An adhesive can be defined as a polymer that can join surfaces and resist their separation [14, 15]. A structural adhesive is one that can resist substantial separating loads, and thus contributes significantly to the strength and stiffness of a structure [14]. The structural elements to be joined are referred to as 'adherends'.

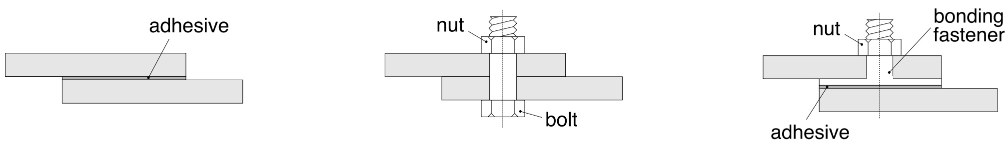

(a) Adhesive bonding (b) Mechanical fastening (c) Hybrid joining

Figure 4: Joining methods investigated

In most cases of mechanical fastening, holes are drilled into the components so that a fastener can be inserted [13]. The most prevalent fasteners are rivets, pins with collars, and bolts with nuts [2]. Pin and collar fasteners can only be used for permanent joints [2], while rivets can cause delamination (separation of the layers of material) in composites during installation [15]. Furthermore, the European Space Agency has stated a preference for bolts when mechanically fastening fibre-reinforced plastic components [16]. Therefore, bolts were the mechanical fastener considered in this work.

Table 1 lists some of the design considerations associated with adhesive bonding and mechanical fastening. In cases where a compromise is sought between the advantages and disadvantages of these joining methods, it is possible to bond a mechanical joining element (or 'bonding fastener') to the surface of a component [13]. This can then be used to join components in a semi-permanent assembly. Despite the apparent utility of bonding fasteners, there is little evidence in the scientific literature of analytical work on this joining technique. Therefore, in addition to adhesive bonding and mechanical fastening, hybrid joining methods were considered in this project.

	Advantages	**Disadvantages**
Adhesive bonding	Adds minimal weight to the structure	Difficult to disassemble without damaging the joint
	Distributes loads over a relatively large area	Relatively sensitive to environmental conditions
	Requires no holes	Difficult to inspect
	Produces smooth external surfaces	Requires surface preparation
Mechanical fastening	Permits quick and repeated disassembly without damaging the joint	Requires machining of holes, interrupting fibre continuity
	Requires little or no surface preparation	Adds significant weight to the structure
	Enables easy inspection	Concentrates stress around the joint
		May introduce corrosion problems

Table 1: Comparison of adhesive bonding and mechanical fastening [1, 2]

Bonding fasteners consist of a mechanical joining element – such as a threaded stud, threaded nut, or pin – connected to a large base plate by welding or clinching (a cold forming technique for joining metals) [17, 18]. Following a review of commercially available products, it was decided that the bonding fastener illustrated in Figure 5 – a threaded stud welded to a perforated steel base – would be used.

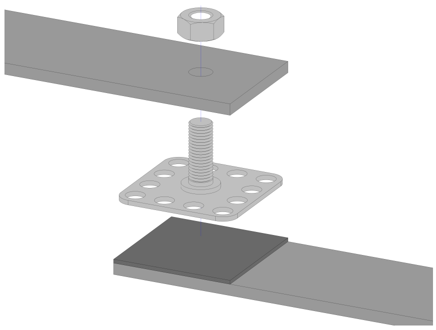

Figure 5: Bonding fastener used to make hybrid joints [17]

This design was selected primarily because it allowed the clearest comparison with adhesive bonding and mechanical fastening. With a square base plate, the bonding area is approximately the same as in an adhesive joint of the same width and overlap length.

With a threaded stud as the mechanical joining element, there is similarity with a conventional conventional bolt and nut assembly.

1.4 Project scope [FBS]

Following the literature review, it was decided that

- Carbon-epoxy laminates would be the considered as the material to be joined
- Three joining methods – adhesive bonding, mechanical fastening, and hybrid joining methods – would be investigated
- Analysis would focus on the mechanical response of joints to static loading

This report describes the theoretical and experimental analyses carried out to characterise the joining methods, leading to a comparison with respect to the requirements of Formula Student.

2 Laminates [FBS]

Before analysing the joining methods it was necessary first to characterise the material to be joined. Carbon-epoxy laminate was procured from an external supplier, ensuring greater consistency in the quality of manufacture than could be achieved by production at the university. Sourcing the material in this way also reduced the time taken to prepare the test specimens, thus allowing more time to conduct an extensive testing programme.

Laminate in two nominal thicknesses – 2mm and 3mm – was used. Both were manufactured by infusing stacked layers of carbon fibre reinforcement with epoxy resin, and consolidating the stack into the desired thickness [21]. In the absence of mechanical testing data from the manufacturer, both theoretical and experimental analyses were carried out to identify the elastic properties and strength of the laminates.

2.1 Theoretical analysis [FBS]

In order to estimate the overall properties of a laminate, its constituent components must be investigated. Table 2 presents the different types of ply (or 'lamina') used in the lay-up of the laminates. The woven fabric plies (types A and C) had a 2/2 twill pattern, produced by weaving the weft fibres alternately over and under two intersecting warps [22]. The type B ply was made by stitching together two unidirectional plies stacked perpendicular to each other. Both types of fabric contained equal proportions of fibres oriented in the weave and weft directions.

The 2mm- and 3mm-thick laminates were composed of 5 and 7 individual plies respec-

Ply type	**Density**	**Form**
A	200gm^{-2}	Woven fabric
B	300gm^{-2}	Stitched non-crimp fabric
C	650gm^{-2}	Woven fabric

Table 2: Types of ply used in the construction of the laminates [21]

tively. Their lay-ups are presented in Table 3.

Laminate type	**1**	**2**	**3**	**4**	**5**	**6**	**7**
2mm	A	B	C	B	A	–	–
3mm	A	B	C	A	C	B	A

Table 3: Ply stacking sequence in the laminates [21]

Figure 6 defines the coordinate system used to describe a laminate and its constituent laminae. The x-, y- and z-axes (the global axes of the laminate) are defined as the 'longitudinal', 'transverse', and 'through-thickness' (also 'interlaminar') directions respectively. In each lamina, the local axes are defined such that the 1-axis runs parallel to the fibres, the 2-axis runs perpendicular to (but in the same plane as) the fibres, and the 3-axis points out-of-plane. All of the ply types used are biaxial, so the lamina 1- and 2-axes are interchangeable.

The orientation, θ, of each lamina is defined as the angle between the 1- and x-axes. The type B plies were stacked at an angle of $\theta = 45°$. This produces laminates with approximately equal fibre reinforcement in the $\theta = 0°$, $\theta = 45°$ and $\theta = 90°$ directions, resulting in quasi-isotropic mechanical properties.

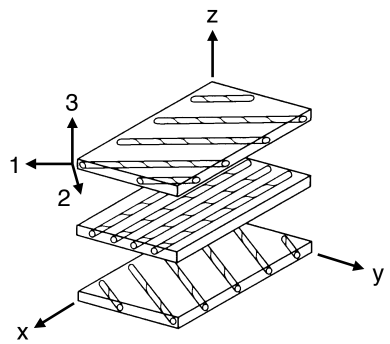

Figure 6: Coordinate system used to describe a laminate (from [23])

2.1.1 Elastic properties [FBS]

Lamina elastic properties, such as tensile modulus (E), Poisson's ratio (ν), and shear modulus (G), are defined with two subscripts. The first denotes the direction of loading, and the second denotes the direction of measurement. For example, ν_{12} represents the ratio of strain in direction 2 to the applied strain in direction 1. Fibre and matrix properties are denoted by f and m subscripts respectively.

The tensile moduli of a lamina can be predicted using a 'rule of mixtures' approach. It is assumed that the lamina property is equal to the weighted sum of the fibre and matrix properties [1]. This requires a definition of V_f, the fibre volume fraction:

$$V_f = \frac{\text{volume of fibres}}{\text{total volume}} \tag{1}$$

For typical woven fabrics, $V_f = 0.5$; for typical non-crimp fabrics, $V_f = 0.6$ [12]. In all ply types, half of the fibres are oriented in the 1-direction, while the other half are oriented in the 2-direction. Therefore, the volume fraction of fibres oriented in either direction is $V_{f1} = V_{f2} = 0.5V_f$.

Using a 'rule of mixtures' approach [1], the longitudinal elastic modulus of each lamina can be expressed as

$$E_{11} = V_{f1}E_f + (1 - V_{f1})E_m \tag{2}$$

The properties of the fibres and matrix [12, 24, 25, 26] can be substituted into Equation 2 for each ply type:

$$\begin{aligned} \text{Types A \& C:} \qquad & E_{11} = (0.25 \times 234) + (0.75 \times 2.4) = 60\text{GPa} \\ \text{Type B:} \qquad & E_{11} = (0.30 \times 230) + (0.70 \times 2.4) = 71\text{GPa} \end{aligned}$$

All ply types had equal proportions of fibres in the 1- and 2-directions. Thus, $E_{11} = E_{22}$. Due to the complex architecture of woven fabrics [35], it was unfeasible within the scope of this project to calculate $\nu_{12} = \nu_{21}$ and G_{12} for each lamina. Instead, typical values were obtained from the literature [12]. These elastic properties can be used to define the stress-strain relation for a lamina in a state of plane stress [1]:

$$\begin{bmatrix} \sigma_{xx} \\ \sigma_{yy} \\ \tau_{xy} \end{bmatrix} = \begin{bmatrix} Q_{11} & Q_{12} & 0 \\ Q_{21} & Q_{22} & 0 \\ 0 & 0 & Q_{66} \end{bmatrix} \begin{bmatrix} \epsilon_{xx} \\ \epsilon_{yy} \\ \gamma_{xy} \end{bmatrix} \tag{3}$$

where the non-zero elements of the stiffness matrix ($\boldsymbol{Q}$) are given by

$$Q_{11} = \frac{E_{11}}{1 - \nu_{12}\nu_{21}} \qquad Q_{12} = Q_{21} = \frac{\nu_{21}E_{11}}{1 - \nu_{12}\nu_{21}} \qquad Q_{22} = \frac{E_{22}}{1 - \nu_{12}\nu_{21}} \qquad Q_{66} = G_{12}$$

The effective elastic properties of the laminates were estimated using The Laminator, an analytical computer program based on the principles of classical lamination theory [28]. The values used as inputs – the elastic properties of the laminae, as well as their thicknesses (t) and orientations (θ) – are presented in Table 4.

Ply type	E_{11} (GPa)	E_{22} (GPa)	G_{12} (GPa)	ν_{12}	t (mm)	θ (°)
A	60	60	3.3	0.1	0.28	0
B	71	71	3.3	0.1	0.35	45
C	60	60	3.3	0.1	0.65	0

Table 4: Lamina elastic properties used to calculate effective laminate properties [12, 21]

Table 5 presents the outputs of the analytical tool. Notably, the calculated thickness is approximately 5% smaller than the nominal thickness in both cases.

Laminate type	E_{xx} (GPa)	E_{yy} (GPa)	G_{xy} (GPa)	ν_{xy}	t (mm)
2mm	49	49	14	0.3	1.91
3mm	53	53	10	0.2	2.84

Table 5: Laminate elastic properties calculated according to classical lamination theory

Classical lamination theory only serves to predict the in-plane properties of a laminate. Determining the through-thickness parameters has historically been more difficult [30]. Since there are no reinforcing fibres oriented in the through-thickness direction, the elastic modulus and Poisson's ratios were assumed to be matrix-dominated (i.e. $E_{zz} = 2.4$GPa and $\nu_{xz} = \nu_{yz} = 0.4$ [12]). Based on an experimental investigation of woven carbon-epoxy laminates by Chan et al [30], the through-thickness shear modulus, $G_{xz} = G_{yz}$, was taken to be 3.2GPa.

2.1.2 Strength [CL]

Tensile loads applied to a lamina are shared between the fibres and the matrix in proportion to their relative volumes:

$$\sigma_A = V_f \bar{\sigma}_f + (1 - V_f)\bar{\sigma}_m \tag{4}$$

where σ_A is the applied stress, V_f is the fibre volume fraction, and $\bar{\sigma}_f$ and $\bar{\sigma}_m$ are the volume-averaged stresses in the fibres and matrix respectively [5]. The same tensile strain is experienced by the fibres and the matrix, leading to the same ratio of stress to Young's modulus. A modified version of Equation 4 can be used to express strength along the longitudinal axis (σ_{1u}):

$$\sigma_{1u} = V_f \sigma_{fu} + (1 - V_f)\sigma_{mu} \tag{5}$$

where σ_{fu} and σ_{mu} are the fibre and matrix strengths respectively. Two failure case can occur. In the first failure case, the matrix has a lower failure strain than the fibres ($\epsilon_{mu} <$

ϵ_{fu}). If the matrix fails independent of the fibres, lamina failure occurs at a strain value of ϵ_{fu} and a stress value of

$$\sigma_{1u} = V_f \sigma_{fu} \tag{6}$$

If the fibres fail before all of the load is tranferred from the matrix, lamina failure occurs at a stress of

$$\sigma_{1u} = V_f \sigma_{fmu} + (1 - V_f)\sigma_{mu} \tag{7}$$

where σ_{fmu} is the stress at which matrix begins to crack. Figure 7a presents stress-strain plots for the fibres and matrix corresponding to this first failure case. Figure 7b shows the relationship between the failure stress of a lamina (σ_{1u}) and the fibre volume fraction (V_f).

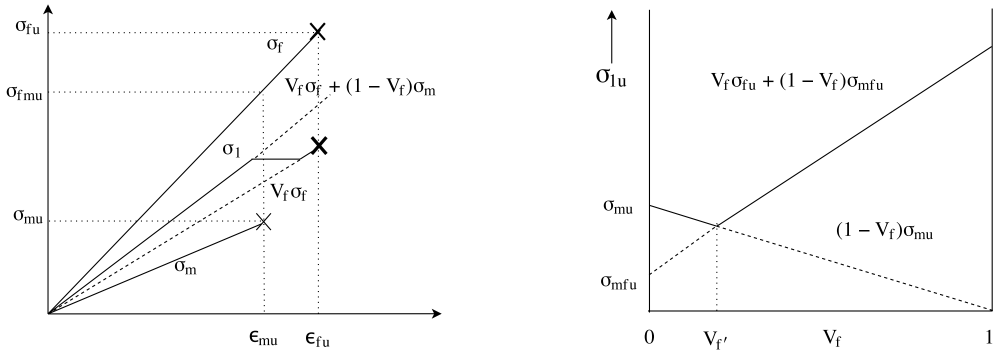

(a) Stress-strain responses of fibres and matrix

(b) Relationship between failure stress and fibre volume fraction

Figure 7: Schematic plots of stress in idealised laminae with $\epsilon_{mu} < \epsilon_{fu}$

In the second failure case, the fibres have a lower failure strain than the matrix ($\epsilon_{fu} < \epsilon_{mu}$). At strains up to ϵ_{fu}, the stress is given by Equation 5. Lamina failure occurs at

$$\sigma_{1u} = (1 - V_f)\sigma_{mu} \tag{8}$$

If the matrix fails while the fibres still bear some load, the failure stress is given by

$$\sigma_{1fu} = V_f \sigma_{fu} + (1 - V_f)\sigma_{mfu} \tag{9}$$

where σ_{mfu} is the stress in the matrix at the onset of fibre cracking.

According to Equation 9, it would be theoretically possible to have a state where the lamina failure stress is lower than that of unreinforced matrix (see dashed line in Figure 8b). This is restricted by a limiting value (V_f') of the fibre volume fraction, which can be found by equating the right hand side of Equation 9 to the right hand side of Equation 8:

$$V_f' = \frac{\sigma_{mu} - \sigma_{mfu}}{\sigma_{fu} - \sigma_{mfu} + \sigma_{mu}} \tag{10}$$

Figure 8a presents stress-strain plots for the fibres and matrix corresponding to the second failure case. Figure 8b shows the relationship between the failure stress of a lamina (σ_{1u}) and the fibre volume fraction (V_f).

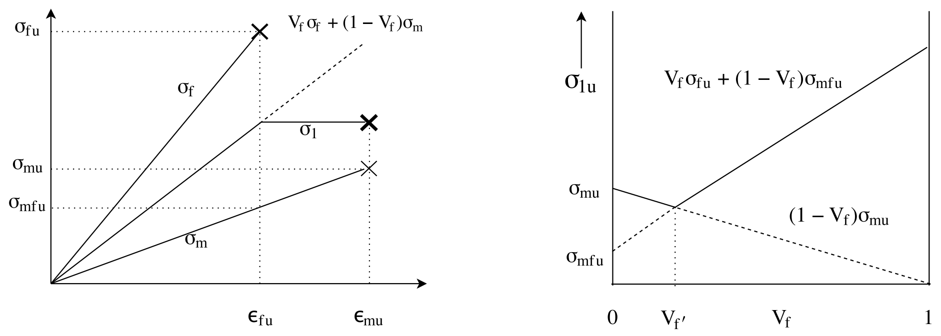

(a) Stress-strain responses of fibres and matrix

(b) Relationship between failure stress and fibre volume fraction

Figure 8: Schematic plots of stress in idealised laminae with $\epsilon_{fu} < \epsilon_{mu}$

Based on the failure strain values found in manufacturers' data sheets [24, 25, 26, 27], it was predicted the failure of the laminates used for this project would correspond to the second failure case ($\epsilon_{fu} < \epsilon_{mu}$). Equations 8-10 were used to calculate the values in Table 6. The uncertainty lay in whether the matrix would fail after load has transferred from the fibres to the matrix (Equation 8), or whether the matrix failure would take place while fibres were still bearing some load (Equation 9).

As described in Section 2.1.1, an analytical computer program was used to estimate the effective properties of the laminates used. The values in Table 6 were used as inputs.

Ply type	σ_{fu}	σ_{mfu}	σ_{mu}	V_f'	V_{f1}	σ_{1fu}	σ_{1mu}
A	4100	21	70	1.2	30	1300	49
B	4900	24	70	0.9	25	1200	52
C	4800	21	70	1.0	30	1500	49

Table 6: Strength-related lamina properties (stresses in MPa; fibre volume fractions expressed as percentages) used to calculate effective laminate properties

Table 7 presents the outputs of the analytical tool, where σ_{1mu} represents the case where only the matrix is still bearing load, and σ_{1fu} where fibres still bear some load at point of failure. Strength predictions are stated according to two failure criteria – the maximum stress criterion, and the Tsai-Hill criterion. Lamina failure criteria can be separated into three groups [87]:

- **Limit criteria** predict failure load and mode by assuming lamina failure when stresses or strains reach critical values in their respective planes. Interaction between axes are ignored.
- **Interactive criteria** assume failure when an equation involving all stress or strain components are satisfied. Single quadratic or higher-order polynomial equations are used. Modes of failures are determined indirectly.
- **Separate mode criteria** distinguish between fibre failure from matrix failure. These mainly differ to limit criteria in that they include interaction between stress com-

ponents.

According to Sun et al [87], maximum stress-strain criteria (types of limit criteria) and the Tsai-Hill interactive criterion are the most commonly used criteria.

Laminate type	σ_{1fu} **(1)**	σ_{1mu} **(1)**	σ_{1fu} **(2)**	σ_{1mu} **(2)**
2mm	660	40	640	36
3mm	770	43	730	41

Table 7: Laminate strength calculated according to (1) maximum stress failure criterion, and (2) Tsai-Hill failure criterion

The maximum stress criterion can be stated in component form [5, 87]:

$$\begin{aligned} \text{Fibre failure:} \quad & \sigma_1 = \sigma_{1u} \\ \text{Matrix transverse failure:} \quad & \sigma_2 = \sigma_{2u} \\ \text{Matrix shear failure:} \quad & \tau_{12} = \tau_{12u} \end{aligned} \tag{11}$$

The dependence on loading angle can be included:

$$\begin{bmatrix} \sigma_1 \\ \sigma_2 \\ \tau_{12} \end{bmatrix} = \begin{bmatrix} c^2 & s^2 & 2cs \\ s^2 & c^2 & -2cs \\ -cs & cs & c^2 - s^2 \end{bmatrix} \begin{bmatrix} \sigma_x \\ \sigma_y \\ \tau_{xy} \end{bmatrix} \tag{12}$$

where $c = \cos(\phi)$ and $s = \sin(\phi)$ respectively, and ϕ is angle between the loading direction and the longitudinal axis of the laminate. Assuming the lamina is under uniaxial loading, the criterion can be written as [85]

$$\begin{aligned} \text{Axial failure:} \quad & \sigma_{xu} = \frac{\sigma_{1u}}{\cos^2(\phi)} \\ \text{Transverse failure:} \quad & \sigma_{xu} = \frac{\sigma_{2u}}{\sin^2(\phi)} \\ \text{Shear failure:} \quad & \sigma_{xu} = \frac{\tau_{12u}}{\sin(\phi)\cos(\phi)} \end{aligned} \tag{13}$$

The maximum strain criterion can be found by substituting the stress components with strain components.

The Tsai-Hill criterion is based on the von Mises criterion for yield in metals, which is given by

$$(\sigma_1 - \sigma_2)^2 + (\sigma_2 - \sigma_3)^2 + (\sigma_3 - \sigma_1)^2 = 2\sigma_Y^2 \tag{14}$$

where σ_Y is the yield strength. Assuming plane stress ($\sigma_3 = 0$), and taking into consideration the anisotropy and failure mechanisms of laminates, the criterion can be re-stated as

$$\left(\frac{\sigma_1}{\sigma_{1Y}}\right)^2 + \left(\frac{\sigma_2}{\sigma_{2Y}}\right)^2 - \left(\frac{\sigma_1\sigma_2}{\sigma_{1Y}^2}\right) - \left(\frac{\sigma_1\sigma_2}{\sigma_{2Y}^2}\right) + \left(\frac{\sigma_1\sigma_2}{\sigma_{3Y}^2}\right) + \left(\frac{\tau_{12}}{\tau_{12u}}\right)^2 = 1 \tag{15}$$

Replacing yield stresses with laminate failure stresses, and setting ($\sigma_{2u} = \sigma_{3u}$) based on transverse isotropy, the Tsai-Hill failure criterion can be stated as

$$\left(\frac{\sigma_1}{\sigma_{1u}}\right)^2 + \left(\frac{\sigma_2}{\sigma_{2u}}\right)^2 - \left(\frac{\sigma_1\sigma_2}{\sigma_{1u}^2}\right) + \left(\frac{\tau_{12}}{\tau_{12Y}}\right)^2 = 1 \tag{16}$$

Compared to the maximum stress criterion, the Tsai-Hill criterion is more conservative [87]. This explains why the Tsai-Hill failure stress values in Table 7 are lower than those predicted by the maximum stress criterion.

2.2 Experimental analysis [FBS]

Mechanical tests of the laminates were carried out according to ASTM D3039 [31]. Specimens of rectangular cross-section were mounted in a universal testing machine and statically loaded in tension.

2.2.1 Specimens and method [FBS]

In this test setup, the tensile load was introduced into the specimen by grips, which clamp the specimen surfaces at each end, and apply a shear force through friction. If smooth grip surfaces were used, the coefficient of friction between the grips and the specimen would be relatively low, and large clamping forces would be required. Laminates have relatively low through-thickness stiffness and strength, so these forces could result in significant compressive stresses and strains. This would reduce the probability of specimen failure in the desired central (non-gripped) region [32]. Therefore, grips with rough surfaces were used, reducing the clamping force required.

Following university standard practice, to avoid damage to the surfaces of the specimen, protective fibreglass tabs of length L_{tab} = 40mm and thickness t_{tab} = 2mm were bonded to the ends of the laminate using epoxy adhesive. Figure 9 illustrates the specimen geometry. The nominal length and width of the specimens were L = 250mm and w = 32mm respectively.

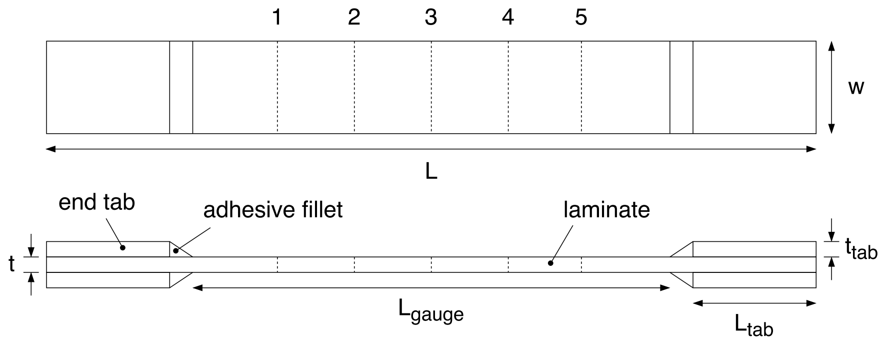

Figure 9: Specimen geometry used in mechanical tests of laminates

Specimens were manufactured by carrying out the following process:

1. Cut the laminate into a sheet of dimensions $L \times nw$ where n is the number of specimens required
2. Grit-blast the strips of tab material and the ends of the laminate sheet to increase surface roughness
3. Clean the laminate and tab material with acetone solvent
4. Apply a layer of adhesive to the grit-blasted area of the laminate
5. Clamp the strips of tab material to the ends of the laminate sheet until the adhesive has cured
6. Cut the sheet into strips of width w

In order to quantify variations that occurred during manufacture, three critical dimensions of each specimen were measured using vernier calipers. The gauge length (L_{gauge}) indicates the longitudinal (length-direction) alignment of the tabs. The width (w) and thickness (t), measured at five points along the gauge length (see Figure 9), were used to calculate the average cross-sectional area of each specimen. Table 8 presents a summary of the measurements, stating mean ($\bar{x}$) and standard deviation (s) values to the resolution of the calipers used (0.01mm).

Laminate type	L_{gauge}	w	t
2mm	159.04 ± 1.13	32.05 ± 0.14	1.90 ± 0.02
3mm	158.37 ± 0.53	31.81 ± 0.21	2.70 ± 0.02

Table 8: Measurements ($\bar{x} \pm s$ in mm) of critical laminate specimen dimensions

Six specimens were tested for each laminate type. Each specimen was mounted in a universal testing machine with its ends clamped by hydraulic grips, which applied a pressure of 20MPa. An engineer's square was used to check the alignment of the specimen in the grips of the machine. The grips were separated longitudinally at a cross-head speed of 2mm/min. The tensile force in the specimen was measured using an 80kN load cell. A video extensometer was used to track the position of 10 marked points on the front face (top view in Figure 9) of the specimen.

2.2.2 Results [FBS]

The average longitudinal direct stress (σ) was calculated by normalising the tensile force (F) with respect to the average specimen cross-sectional area before loading ($\bar{A}$) [31]:

$$\sigma = \frac{F}{\bar{A}} \tag{17}$$

where

$$\bar{A} = \frac{1}{5}\sum_{i=1}^{5} w_i t_i$$

The average longitudinal direct strain (ϵ) was calculated by finding the change in distance (Δ) between pairs of tracked points, and normalising with respect to the original distance (L_0) [31]:

$$\epsilon = \frac{\Delta}{L_0} \tag{18}$$

Figure 10 shows the engineering stress-strain curves plotted using the experimental results.

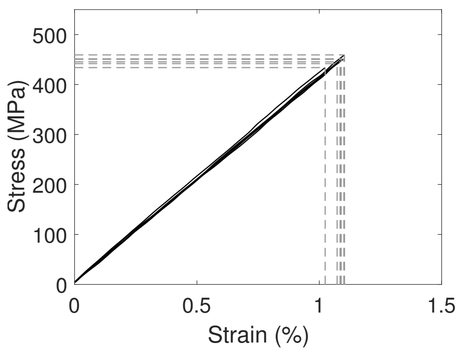

(a) 2mm nominal thickness

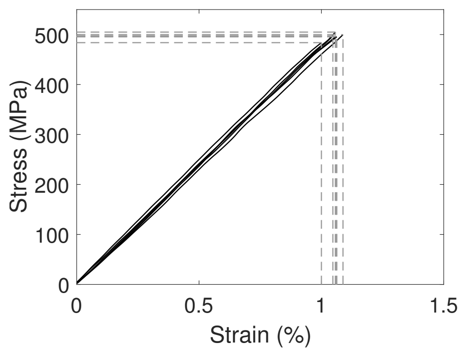

(b) 3mm nominal thickness

Figure 10: Experimentally determined longitudinal stress-strain responses of laminates

The longitudinal tensile modulus (E_{xx}) was calculated using the stress values at $\epsilon = 0.1\%$ and $\epsilon = 0.3\%$. The difference between the stress values was divided by the strain range to give E [31]:

$$E_{xx} = \frac{\sigma_{0.003} - \sigma_{0.001}}{0.003 - 0.001} \tag{19}$$

The in-plane Poisson's ratio (ν_{xy}) was calculated by dividing the change in transverse (width-direction) strain (ϵ') by the same longitudinal strain range:

$$\nu_{xy} = \frac{\epsilon'_{0.003} - \epsilon'_{0.001}}{0.003 - 0.001} \tag{20}$$

Table 9 presents sample mean and standard deviation values for the material properties of interest. The sample mean was calculated as

$$\bar{x} = \frac{1}{n}\sum_{i=1}^{n} x_i \tag{21}$$

where x_i is a given measured or derived property, and n is the sample size [31]. The sample standard deviation was found using

$$s = \sqrt{\frac{1}{n-1}\left[\left(\sum_{i=1}^{n} x_i^2\right) - n\bar{x}^2\right]} \tag{22}$$

The values of ultimate longitudinal direct strength (σ_u) and strain (ϵ_u) correspond to the values of engineering stress and strain respectively at failure.

Laminate type	σ_u **(MPa)**	ϵ_u **(%)**	E_{xx} **(GPa)**	ν_{xy}
2mm	447.08 ± 8.77	1.08 ± 0.03	41.09 ± 1.04	0.29 ± 0.06
3mm	496.33 ± 6.99	1.05 ± 0.03	47.07 ± 1.54	0.14 ± 0.04

Table 9: Experimentally determined laminate material properties ($\bar{x} \pm s$)

In order to verify the statistical significance of the values used to calculate $\bar{x}$ and s in Table 9, Peirce's criterion [33] was applied. This criterion was found by Ross [34] to be more rigorous than the commonly used Chauvenet criterion. For each measured or derived property (x_i) the deviation from the sample mean ($x_i - \bar{x}$) is calculated. If the magnitude of this deviation exceeds a critical value ($|x_i - \bar{x}|_{max}$), then the data point can be classed as an outlier. This critical value is given by

$$|x_i - \bar{x}|_{max} = Rs \tag{23}$$

where R is a parameter retrieved from a reference table, and s is the sample standard deviation. This test was carried out using the ultimate tensile strength and strain values for each sample. Three samples in total were found to produce outlying results – two from the 2mm laminate set, and one from the 3mm laminate set. The sample mean and standard deviation were recalculated, omitting the outliers. Table 10 shows the adjusted values.

Laminate type	σ_u **(MPa)**	ϵ_u **(%)**	E_{xx} **(GPa)**	ν_{xy}
2mm	447.32 ± 4.48	1.09 ± 0.01	40.79 ± 0.85	0.30 ± 0.06
3mm	498.83 ± 3.76	1.06 ± 0.02	46.58 ± 1.08	0.13 ± 0.03

Table 10: Experimentally determined laminate material properties ($\bar{x} \pm s$) after eliminating outliers

2.3 Discussion [FBS]

The predictions of the theoretical analysis are compared with the experimental results. Potential sources of variation in experimental results are identified, and ways of mitigating variation are suggested. A reflection is made on the value and validity of the analyses carried out.

2.3.1 Comparison of elastic property predictions with results [FBS]

The experimentally determined values for the longitudinal elastic modulus (E_{xx}) were 10-15% smaller than the theoretical predictions. It is suggested that this difference is a result of over-idealing the laminae. The estimations were based on a number of assumptions [1]:

- The fibres and the matrix are linearly elastic, isotropic materials
- The fibres are uniformly distributed in the matrix
- The fibres are perfectly aligned in the 1- and 2-directions
- There is perfect bonding between the fibres and the matrix
- The lamina is free of voids

Even with strict quality control in production, this set of assumptions is unlikely to reflect the components of the laminates tested. In addition, Equation 2 neglects the effect of the transversely loaded fibres on the stiffness of the laminae.

Common to both analyses was that the 3mm laminate had a greater elastic modulus than the 2mm laminate. This can be explained with reference to their lay-ups (see Table 3). The 3mm laminate contained proportionately more fibre reinforcement in the x-direction: five of its seven plies are oriented at $\theta = 0°$, compared to three out of five plies in the 2mm laminate.

The in-plane Poisson's ratios of the laminates differ for the same reason: with proportionately more fibres oriented in the $\theta = 90°$ direction, the 3mm laminate provides greater resistance to transverse contractions than the 2mm laminate, resulting in a lower ν_{xy} value. For the 2mm laminate, there was good agreement between the experimentally and theoretically determined values of in-plane Poisson's ratio (ν_{xy}). However, with for the 3mm laminate, the experimental value was 35% lower than the theoretical prediction.

2.3.2 Comparison of strength predictions with results [CL]

The experimental results suggest that the laminates failed while fibres were still bearing some load: the failure stresses were closer to σ_{1fu} than σ_{1mu} (see Table 7). The results for the longitudinal strength (σ_{1u}) were 40-55% smaller than the theoretical predictions. This difference can be explained with a consideration of the simplifications of the theoretical models.

The theoretical predictions were based on analysis of unidirectional plies, whereas the laminates tested had a combination of 2-2 twill woven and non-crimp fabric plies. With additional bending stresses in the crimps of the woven fibre architecture, axial strengths are likely to have been overestimated.

Another assumption was that the transversely loaded fibres do not contribute to overall strength of the ply. As suggested by Hull and Clyne [5], the transversely loaded fibres can be modelled as cylindrical holes. Hence, the load-bearing cross-section is reduced. A simplified expression for estimating transverse strength is

$$\sigma_{2u} = \sigma_{mu}\left[1 - 2\left(\frac{V_f}{\pi}\right)^{1/2}\right] \tag{24}$$

It can be seen that the strength of transversely loaded fibres is lower than the strength of the matrix alone. Paiva et al [88] investigated the mechanical properties of various woven architectures, and found that plain woven laminates are approximately 53% weaker than unidirectional laminates in the longitudinal direction. The 2-2 twill weave pattern causes reduced crimp compared to the plain weave pattern [22], which should result in greater strength.

The analysis was based on a number of other significant simplifications. While fibres still bear some load after failure, this was not included. The redistribution of stress after fibres fracture was neglected. The fibres were assumed to be of constant length, and were assumed to fail independently of one another.

In addition, the constituent materials of a lamina were over-idealised. Carbon fibres are typically brittle, failing without extensive plastic deformation. Their actual strength is typically significantly lower than theoretical values. This is because they contain microscopic flaws, which are randomly distributed along the length of the fibre. For this reason, statistical approaches are generally used to predict the strength of carbon fibres. By dividing up the length of the fibre into small sections, n_σ can be used to describe the number of flaws per unit length sufficient to cause failure. A fibre will fail when any of its sections exhibits a flaw. The probability of failure in the ith segment is given as

$$P_{fi} = n_\sigma \Delta L_i \tag{25}$$

Adding up the sections, and by the approximation of $(1-x) \approx \exp(-x)$ the probability of survival for the entire fibre is given by [85]

$$P_s = \exp\left[-\left(\mathrm{P_{f1}} + \mathrm{P_{f2}} + \cdots + \mathrm{P_{f}}_N\right)\right] \tag{26}$$

Combined with Weibull's theory of failure in brittle materials, the probability of failure in a fibre is

$$P_s = 1 - \exp\left[-\left(\frac{L}{L_0}\right)\left(\frac{\sigma}{\sigma_0}\right)^m\right] \tag{27}$$

where m is the Weibull modulus, and σ_0 is the most probable strength from a fibre length L_0. A lower modulus gives more uncertainty in the variation of fibre strengths. Typical Weibull moduli of fibres are 2-15 [5].

2.3.3 Variation in results [FBS]

The existence of outliers in the experimental results could reasonably be attributed to variations in the production of specimens. Particularly notable were the visible geometric inconsistencies introduced when cutting the specimens to size. Additionally, variations in the shape and size of the adhesive fillets are likely to have affected the stress distribution in the specimens. These manufacturing errors were difficult to avoid given the lack of experience of the workers. Indeed, it was found that specimen quality improved with practice, suggesting that skill level did have an effect on process variability. The specimens were produced in batches, so it is suggested that no skill-related variations occurred within each set of specimens.

It is stated in ASTM D3039 that the use of protective end tabs is not a strict requirement for multidirectional laminates [31]. Given that the application of end tabs introduced more variability in the geometry of the specimens, using specimens without end tabs may have produced more consistent results. However, it could not be ensured that the clamping pressure would not lead to excessive crushing of the laminates, so it was decided that end tabs should be used. Future workers may attempt to investigate whether non-tabbed specimens fail (with reasonable frequency) at acceptable locations and with appropriate failure modes. If non-tabbed specimens are found to produce more consistent results, the time taken to produce tensile specimens could be greatly reduced.

2.3.4 Evaluation of analyses [FBS]

Both analyses provided some insight into the in-plane behaviour of laminates, returning elastic property and strength values similar to those found in the literature for carbon-epoxy laminates [1, 12, 29]. The theoretical predictions were comparable to the experimental results, and could be used for preliminary estimates in the design process.

Refining the models further could produce better agreement with experimental results. Particular attention should be paid to the effect of a woven fibre architecture on the mechanical properties of laminates, as discussed by Crookston et al [35] in their review of analytical models. In order to provide a more complete understanding of these materials, the analysis should provide predictions for out-of-plane (through-thickness) properties in addition the in-plane properties investigated here. Any predictions made should be compared with experimentally determined results, which can be obtained using the methods summarised in ASTM D4762 [36].

3 Adhesive bonding [FBS]

Figure 11 shows typical configurations of adhesive joints. The adherends (parts being joined) are typically loaded in tension. The resultant loads on the adhesive are a function of the geometry of the joint [14]. In cases where the adherends are relatively thin, the dominant loading modes are those shown in Figure 12 [37]. Joints tend to be designed to avoid significant tensile loading of the adhesive, which usually has a low strength compared to the materials being joined [23]. Hence, lap joints, in which the adhesive layer deforms primarily in shear, are widely used.

The single lap joint is the configuration most comprehensively covered in the literature, and most often used for testing adhesives [14]. Kinloch [38] attributes this to the simplicity of the design – and, hence, widespread use in industry – as well as the relative convenience the geometry affords in manufacturing test specimens. Simplicity in design, assembly and testing are important design criteria in Formula Student (see Section 6.3), so single lap joints were considered for this project.

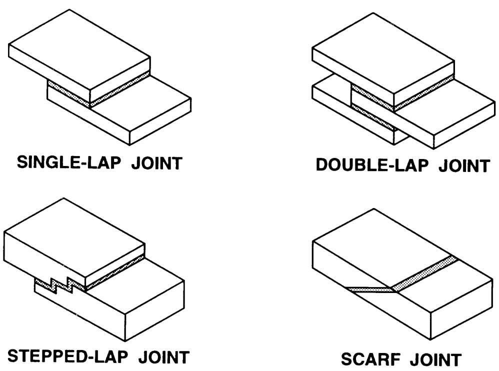

Figure 11: Adhesive joint configurations commonly used in engineering (from [23])

The design of adhesive joints should be based on predictions of the stresses that can be expected during operation. These can be determined theoretically using closed-form solutions or finite element analysis. The former are algebraic expressions that can be used to make simple, fast estimations; the latter is more sophisticated, enabling the use of more refined material models and more complex geometry. Combined with an appropriate failure criterion, this information can be used to predict the loading limits of a joint [39, 40].

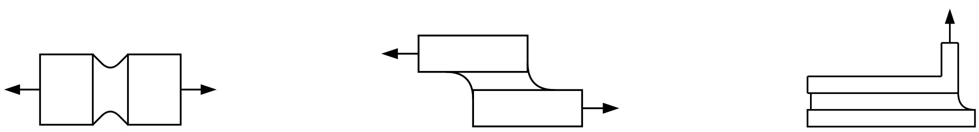

(a) Tension (b) Shear (c) Peel

Figure 12: Adhesive loading modes in joints between fibre-reinforced plastics

Theoretical stress predictions were made. Failure modes and a failure criterion were identified. Based on the closed-form analysis, an investigation was made into the effects of varying the geometric parameters of a joint. Finally, an experimental testing programme was carried out.

3.1 Stress prediction by closed-form analysis [FBS]

Figure 13 defines the coordinate system and dimensions used to describe a single lap adhesive joint. Two adherends of equal width, w, and of thickness t_t (top) and t_b (bottom), are joined by an adhesive layer of length L and thickness t_a. A tensile load (F) is applied to the adherends. The adherends are assumed to have the same elastic modulus (E), shear modulus (G) and Poisson's ratio (ν). The adhesive elastic properties are denoted by a subscripts. The x-, y- and z-axes are referred to as the 'longitudinal', 'through-thickness', and 'transverse' directions respectively.

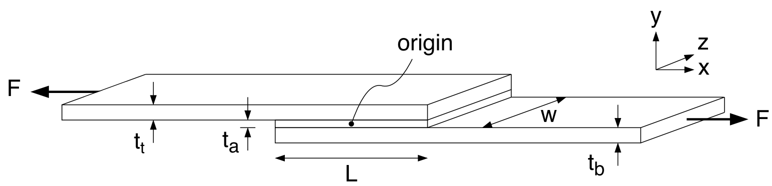

Figure 13: Schematic diagram of a single lap adhesive joint

The plots presented in this section of the report were produced using parameter values sourced from existing literature on adhesive joints [14, 40] (see Table 11). These plots serve two purposes. First, they illustrate the predicted stresses in the adhesive layer. Second, they validate the MATLAB [41] programs written to implement the closed-form solutions. By comparing the plots in Figures 15, 17, 18 and 20 to those in the literature, it can concluded that no errors were made in translating the mathematical expressions to computer code.

w	L	t	t_a	E	G	ν	E_a	G_a	F
25.4	12.7	1.62	0.25	70	25	0.3	4.82	1.72	1000

Table 11: Values of adhesive joint parameters (geometry in mm; elastic and shear moduli in GPa; force in N) used in Section 3.1

3.1.1 Rigid adherend analysis and Volkersen's analysis [FBS]

The simplest analysis of single lap joints considers the adhesive as a linear elastic solid that can only deform in shear [14, 38]. The adherends are considered first as rigid (inextensible) bodies, and then as elastic. In both cases, referring to Figure 16, the tensile load in the top adherend is greatest at $x = -L/2$, where it bears the full load, F. The load decreases linearly to zero at $x = L/2$, where there is a free surface. Similarly, the load in the bottom adherend falls from F at $x = L/2$ to zero at $x = -L/2$.

In the first case, the adherends do not deform under loading, and the adhesive layer is subjected to uniform shear strain (note the regular parallelogram shape of the deformed adhesive elements in Figure 14b). Thus, the longitudinal shear stress, τ_0, in the adhesive is constant:

$$\tau_0 = \frac{F}{wL} \tag{28}$$

Despite the significant limitations of this model, it is the basis for quoting adhesive shear strength according to ASTM standards [40].

Volkersen [42] considered elastic adherends. In this case, the strain in the adherends is proportional to the tensile load. Thus, the strain in the top adherend decreases progressively from $x = -L/2$ to zero at $x = L/2$ (points A and B respectively in Figure 14c).

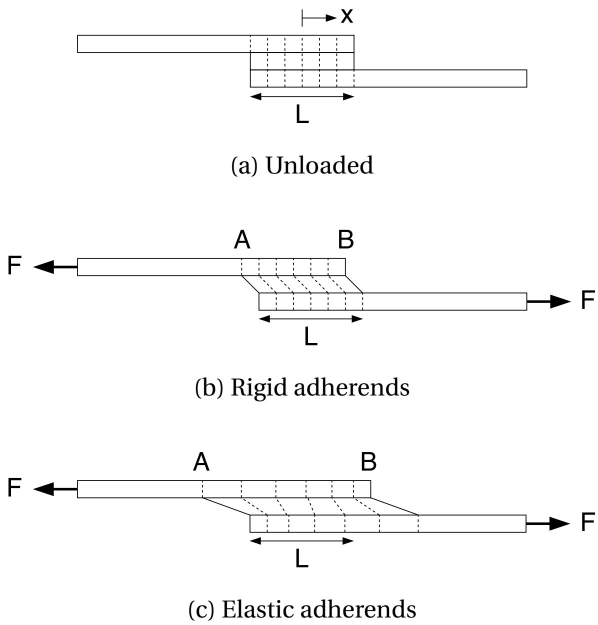

Figure 14: Development of Volkersen's analysis of adhesive joints

The nonlinear adherend strain along the overlap, combined with the continuity of the adhesive-adherend interface, causes non-uniform ('differential') shear stress and strain in the adhesive layer [40], as illustrated by the irregular shapes of the deformed elements in Figure 14c. Volkersen's prediction of the longitudinal shear stress in the adhesive is given by

$$\tau_V = \tau_0 \left[\frac{\omega}{2} \frac{\cosh(\omega X)}{\sinh(\omega/2)} + \left(\frac{\psi - 1}{\psi + 1} \right) \frac{\omega}{2} \frac{\sinh(\omega X)}{\cosh(\omega/2)} \right] \tag{29}$$

where

$$\omega = \sqrt{\phi(1+\psi)} \qquad \psi = \frac{t_t}{t_b} \qquad \phi = \frac{G_a L^2}{E t_t t_a} \qquad X = \frac{x}{L}$$

E is the adherend Young's modulus, G_a is the adhesive shear modulus, and x is the longitudinal coordinate (with origin in the middle of the overlap) [14]. Shear stress is predicted to be maximum at the ends of the overlap, and significantly lower in the middle of the joint, as shown in Figure 15.

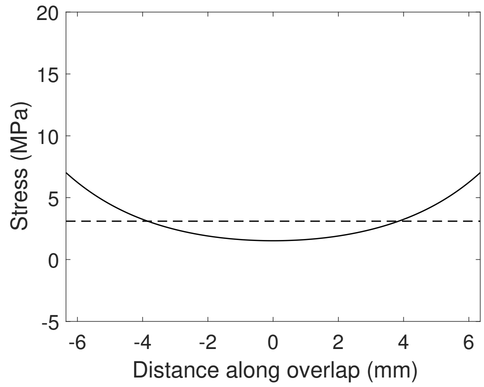

Figure 15: Adhesive shear stress distribution predicted by the rigid adherend model (τ_0 – dashed) and the Volkersen model (τ_V – solid)

3.1.2 Goland and Reissner's analysis [FBS]

While Volkersen's solution corresponds well with double lap joints, it omits physical effects too significant to neglect in single lap joints. The first to consider these effects were Goland and Reissner [43], who noted that the forces applied to the two adherends are not collinear. The resultant eccentric load path causes a bending moment and a through-thickness transverse force to be applied to the joint in addition to the tensile load (Figure 16a). The bending moment, combined with the flexibility of the adherends, leads to rotation of the joint, changing the geometry to align the tensile forces more closely (Figure 16b).

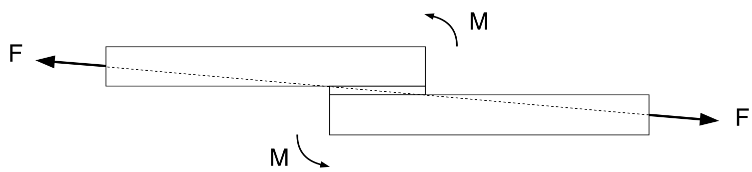

(a) Undeformed joint

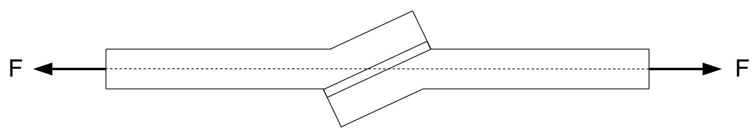

(b) Deformed joint

Figure 16: Bending effect of eccentric loading in single lap joints

Goland and Reissner accounted for the rotation of the joint by using a bending moment factor, k. This relates the bending moment on the adherend at the end of the overlap, M, to the applied load, F [14]:

$$M = kF\frac{t}{2} \tag{30}$$

where $t = t_t = t_b$ is the adherend thickness. At low loads, as in Figure 16a, joint rotation is small, the loading path is highly eccentric, and $k \approx 1$. The deformation of the joint at higher loads reduces the eccentricity and, thus, the value of k.

Goland and Reissner considered two limiting cases for finding the stresses in the adhesive layer [38, 40]:

1. Where the adhesive layer is relatively inflexible, and the joint is treated as a single body with the same material properties as the adherends
2. Where the deformation of the adhesive layer contributes significantly to the stress distribution in the joint

The second approximation is more appropriate for fibre-reinforced plastic adherends [23]. The adhesive layer is treated as an infinite number of shear springs and an infinite number of tension/compression springs in the y-direction (through-thickness) [14]. Solving the differential equations that describe this system yields the following expression for the adhesive shear stress [14, 44]:

$$\tau_{GR} = \frac{\tau_0}{4}\left[(1+3k)\frac{\beta c}{t}\frac{\cosh\big((\beta c/t)(x/c)\big)}{\sinh(\beta c/t)} + 3(1-k)\right] \tag{31}$$

where $\bar{F}$ is the applied load per unit width, c is half the overlap length, and, for adherends of Poisson's ratio ν,

$$\beta = \sqrt{\frac{8G_a t}{Et_a}} \qquad k = \frac{1}{1+2\sqrt{2}\tanh(u)} \qquad u = \frac{L}{2}\sqrt{\frac{3\bar{F}(1-\nu^2)}{2Et^3}}$$

As a result of the bending of the adherends, peel stresses are induced in the adhesive. These are direct stresses that act in the through-thickness direction. Their magnitude is given as [14, 44]

$$\begin{aligned}\sigma_{GR} =& \frac{\bar{F}t}{c^2R_3}\left[\left(R_2\lambda^2\frac{k}{2} + \lambda k'\cosh(\lambda)\cos(\lambda)\right)\cosh\left(\frac{\lambda x}{c}\right)\cos\left(\frac{\lambda x}{c}\right)\right.\\ &\left.+\left(R_1\lambda^2\frac{k}{2} + \lambda k'\sinh(\lambda)\sin(\lambda)\right)\sinh\left(\frac{\lambda x}{c}\right)\sin\left(\frac{\lambda x}{c}\right)\right]\end{aligned} \tag{32}$$

where

$$\lambda = \frac{c}{t}\sqrt[4]{\frac{6E_a t}{Et_a}} \qquad k' = \frac{kc}{t}\sqrt{\frac{3\bar{F}(1-\nu^2)}{Et}}$$

and

$$\begin{aligned}R_1 &= \cosh(\lambda)\sin(\lambda) + \sinh(\lambda)\cos(\lambda)\\ R_2 &= \sinh(\lambda)\cos(\lambda) - \cosh(\lambda)\sin(\lambda)\\ R_3 &= \tfrac{1}{2}\big(\sinh(2\lambda) + \sin(2\lambda)\big)\end{aligned}$$

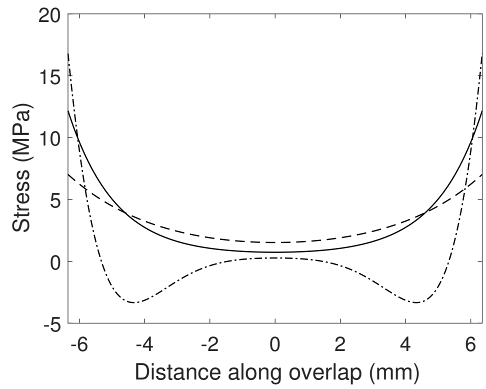

Figure 17: Adhesive shear stress distribution predicted by the Volkersen model (τ_V – dashed) and the Goland and Reissner model (τ_{GR} – solid); peel stress distribution predicted by the Goland and Reissner model (σ_{GR} – dashed/dotted)

Figure 17 compares Goland and Reissner's predictions with those of Volkersen. Both Hart-Smith [45] and Zhao et al [46] presented alternative expressions for the bending moment factor (k) used in Equations 30-32. Hart-Smith aimed to improve the validity of the stress prediction, while Zhao et al provided a simpler expression for k [14]. A comparison of plots of Goland and Reissner's predictions with Hart-Smith's predictions revealed only minor differences. Furthermore, Zhao et al found that their solution was only comparable in accuracy to Goland and Reissner's for a limited range of parameter values [14]. Therefore, it was decided that Goland and Reissner's expression for k would be used.

3.1.3 Allman's analysis [FBS]

A notable limitation of the work of Volkersen, Goland and Reissner is that it predicts non-zero shear stress at the ends of the overlap. This implies a complementary shear stress at a free surface, which violates the boundary condition. Benson [47] identified this as the result of neglecting the through-thickness variation of peel stress in the adhesive [48]. Allman [49] addressed this, deriving the following expression for the shear stress distribution in the adhesive layer:

$$\tau_A = \tau_0 \Bigg[(1-r) + \omega_1 \left(\frac{1 + r(\omega_2 c - 1)}{\omega_2 - \omega_1 \coth(\omega_1 c)} \right) \frac{\cosh(\omega_1 x)}{\sinh(\omega_1 c)} - \omega_2 \left(\frac{1 + r\big(\omega_1 c \coth(\omega_1 c) - 1\big)}{\omega_2 - \omega_1 \coth(\omega_1 c)} \right) e^{-\omega_2 (c-x)} \Bigg] \tag{33}$$

where

$$r = \frac{2cP}{\bar{F}t} \qquad P = \tau_0 t \left[\frac{1 + 3k(1+\epsilon)^2}{1 + 3(1+\epsilon)^2} \right] \qquad \epsilon = \frac{t_a}{t}$$

and c and k are defined as in Goland and Reissner's equations. The expressions for ω_1 and ω_2 depend on the joint parameters. For Allman's example with fibre-reinforced plastic adherends,

$$\omega_1 = \frac{0.6067}{t} \qquad \omega_2 = \frac{4.9119}{t}$$

For the same example, the peel stress distribution is described by

$$\sigma_A = \frac{\tau_0 t}{2}(1+\epsilon)\left[\omega_4^2\left(\frac{1-k+kc\omega_3\tanh(\omega_3 c)}{\omega_4-\omega_3\tanh(\omega_3 c)}\right)e^{-\omega_4(c-x)} - \omega_3^2\left(\frac{1-k+kc\omega_4}{\omega_4-\omega_3\tanh(\omega_3 c)}\right)\frac{\cosh(\omega_3 x)}{\cosh(\omega_3 c)}\right] \tag{34}$$

where

$$\omega_3 = \frac{0.5426}{t} \qquad \omega_4 = \frac{1.8582}{t}$$

As shown in Figure 18, in contrast with the Goland and Reissner model, Allman's model predicts zero shear stress at the ends of the overlap, thus satisfying the free boundary condition.

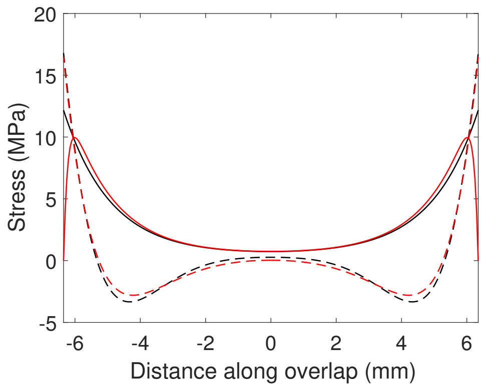

Figure 18: Adhesive shear stress (solid) and peel stress (dashed) distributions predicted by the Goland and Reissner (black) and Allman (red) models

3.1.4 Adams and Peppiatt's analysis [FBS]

All of the models discussed thus far have been based on a plane strain assumption, considering the joint to be sufficiently wide to neglect stresses and strains in the z-direction, thus giving a two-dimensional (x-y) problem. An investigation by Adams and Peppiatt [50] revealed that, in fact, Poisson's ratio strains do have some effect.

Their predictions were based on a simple physical argument [14]. Consider point B in Figure 19. In the top adherend, a uniform tensile load up to point B results in uniform contraction in width and thickness due to Poisson's ratio. In the bottom adherend, however, the tensile load is zero, so there will be no transverse contraction. This situation could exist if the adhesive had zero shear stiffness. In reality, the transverse contraction of the top adherend is restrained by the adhesive, inducing tensile stresses in the width direction.

Bending effects were not considered by Adams and Peppiatt, so their prediction for the longitudinal shear stress distribution is essentially the same as Volkersen's. Approximate

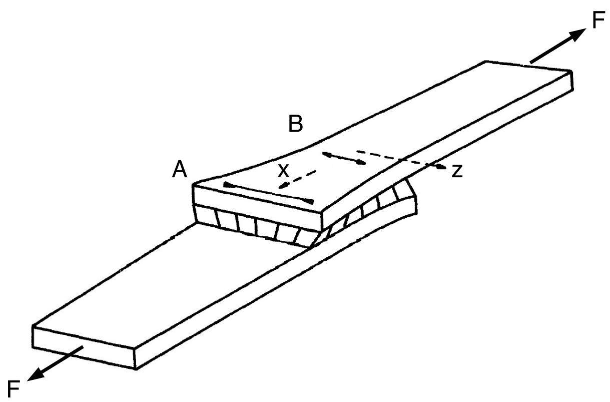

Figure 19: Transverse deformations in a single lap joint due to Poisson's ratio effects (from [14])

solutions for the z-direction (in-plane transverse) stresses are plotted in Figure 20. It can be seen from these graphs that the transverse stresses, although not zero, are small relative to the longitudinal stresses shown in, for example, Figure 15. Indeed, da Silva et al [40] suggest that two-dimensional analysis is satisfactory for most cases.

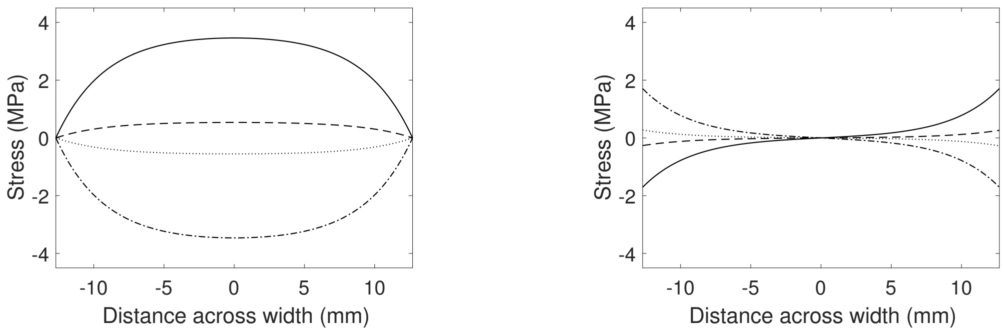

(a) Direct stress in top adherend

(b) Shear stress in adhesive

Figure 20: Transverse stresses predicted by Adams and Peppiatt at
$x = -L/2$ (solid), $x = -L/4$ (dashed), $x = L/4$ (dotted), and $x = L/2$ (dashed-dotted)

3.2 Stress prediction by finite element analysis [FBS]

The closed-form models discussed in Section 3.1 assume linear elastic and isotropic materials. This limits their validity for laminate adherends, which are strongly anisotropic. Finite element analysis software allows more appropriate material models to be used. In Abaqus [52], which was used for this work, orthotropic materials (those with three orthogonal planes of material property symmetry [1]) can be defined by nine constants – three elastic moduli (E_{11}, E_{22}, E_{33}), three Poisson's ratios (ν_{12}, ν_{13}, ν_{23}), and three shear moduli (G_{12}, G_{13}, G_{23}). The subscripts have the same meaning as in Section 2.1: the first number denotes the direction of loading, and the second denotes the direction of measurement.

In order to model the 2mm nominal thickness laminate discussed in Section 2.1, the theoretically predicted in-plane elastic properties (see Table 5) were used in conjunction with out-of-plane properties sourced from the literature (see Section 2.1). Table 12 presents these values.

E_{11}	E_{22}	E_{33}	ν_{12}	ν_{13}	ν_{23}	G_{12}	G_{13}	G_{23}
49	49	2.4	0.3	0.4	0.4	14	3.2	3.2

Table 12: Laminate material properties (moduli in GPa) used in finite element analysis

3.2.1 Validation of material model [FBS]

Before investigating an adhesive joint, a validation case was carried out to check that the material model was appropriate. A finite element model was created to represent the tensile tests described in Section 2.2 (see Figure 21). The specimen was approximated by a cuboid of length L = 250mm, width w = 32mm and thickness t = 1.9mm. The 40mm-long end regions were partitioned in order to apply boundary conditions simulating the role of the testing machine grips. One end (A) was constrained in all degrees of freedom. The other end (C) was constrained in all degrees of freedom except for longitudinal translation, which was assigned a displacement value of Δ = 2mm to represent the moving grips of the testing machine.

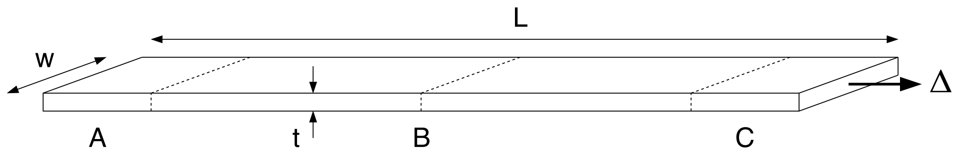

Figure 21: Schematic of the finite element model used for validation of the laminate material model

The maximum principal stress (σ_{max}) and maximum principal strain (ϵ_{max}) were found for each element lying on the midpoint (B) of the specimen. Using an initially coarse mesh (approximate global element size, e = 32mm), the average stress and strain values in this element set were calculated. These average values were plotted against the inverse of element size for progressively more refined meshes (halving e each iteration to a minimum value of 1mm), as shown in Figure 22. Standard 8-node linear brick elements were judged to be suitable because the model was geometrically simple as well as linear elastic.

Shown in Figure 22 are values of stress and strain estimated (to four significant figures) using simple closed-form expressions. For strain,

$$\epsilon_{max} = \frac{\Delta}{L_0} = \frac{2}{250-(2\times 40)} = 1.176\% \tag{35}$$

where L_0 is the original gauge (non-gripped) length of laminate [53]. For stress,

$$\sigma_{max} = E\epsilon_{max} = 48{,}800 \times 0.01176 = 574.1\text{MPa} \tag{36}$$

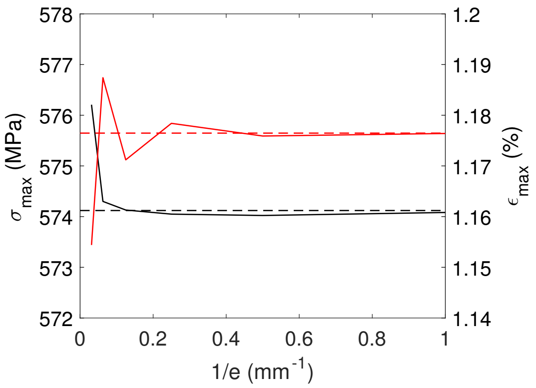

Figure 22: Convergence of maximum principal stress (solid black) and strain (solid red) finite element predictions with closed-form solutions (dashed) with increasing mesh refinement

where $E = E_{11}$ [53]. Compared to the predictions made with e = 2mm, the stress and strain values returned using e = 1mm changed by less than 0.1%, suggesting a convergence of the solution. The finite element solutions for σ_{max} and ϵ_{max} were within 0.1% of the closed-form predictions. Thus, it was concluded that the material model was implemented correctly. Figure 23 shows the mesh with an element size of e = 2mm.

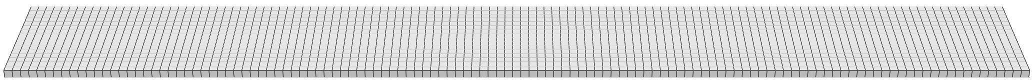

Figure 23: Mesh used in finite element analysis of a laminate tensile specimen

Figure 24 shows the deformation of and stress distribution in the finite element model.

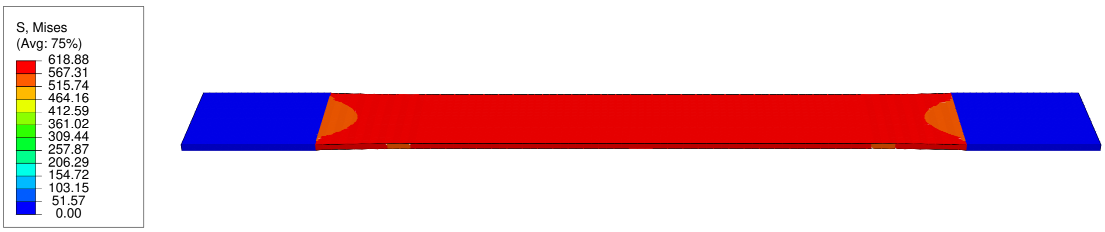

Figure 24: Deformed shape and stress distribution (in MPa) predicted by finite element analysis of a laminate tensile specimen

3.2.2 Adhesive joint [FBS]

A finite element model of the single lap joint used for experimental testing (see Section 3.4) was made. The adherends were approximated by cuboids of length L_{lam} = 145mm, width w = 16mm and thickness t_{lam} = 1.9mm. This width is half that of the specimen being modelled. By using a boundary condition to represent the plane of symmetry at the mid-width, the finite element model was halved in size, thus reducing the computing time for each simulation.

An overlap length of L = 32mm and an adhesive thickness of t_a = 0.1mm were used. As in the validation case, 40mm-long end regions were partitioned in order to apply boundary conditions simulating the role of the testing machine grips. One end (A) was constrained in all degrees of freedom. The other end (B) was constrained in all degrees of freedom except for longitudinal translation, which was assigned a displacement value of Δ = 1mm to represent the moving grips of the testing machine. The material parameters stated in Table 12 were used for the adherends. Typical elastic properties of epoxy resin (E = 2.4GPa and ν = 0.4 [12]) were used for the adhesive.

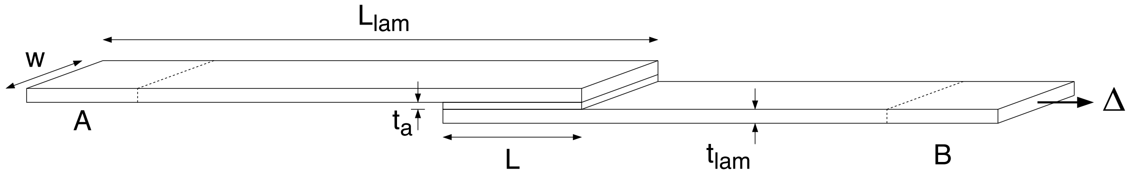

Figure 25: Schematic of the finite element model used to investigate an adhesive joint

A mesh convergence study was carried out in order to find a mesh density that satisfactorily balanced accuracy with computing speed. As in the validation case, standard 8-node linear brick elements were judged to be suitable because the model was geometrically simple as well as linear elastic.

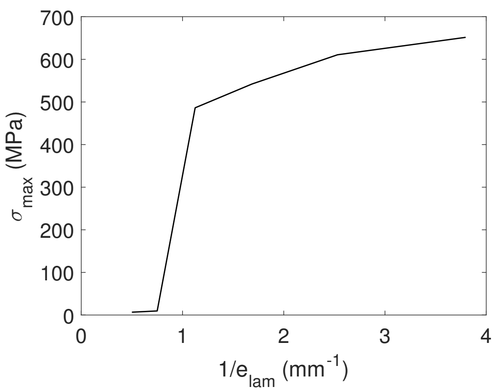

Figure 26: Convergence of maximum von Mises stress finite element predictions with increasing mesh refinement

A constant length ratio was used between the size of the laminate elements (e_{lam}) and the size of the adhesive elements (e_a): $e_{lam} = 5e_a$. Using the same element size throughout the model would have been problematic. With a coarse mesh, the aspect ratio (ratio of longest edge length to shortest edge length) of the adhesive elements would have been large, potentially reducing the accuracy of the analysis [54]. With a fine mesh, due to the size of the adherends, the number of elements would have been large, resulting in significant computing time to complete the analysis.

Using an initially coarse mesh (e_{lam} = 2mm), the maximum von Mises stress (σ_{max}) in the model was found. Reducing the element size by a factor of 1.5 with each iteration, the simulation was run an additional five times. Figure 26 shows a plot of the maximum stress prediction against the inverse of e_{lam} for each of the simulations. Figure 27 shows the mesh with element sizes of $e_{lam} = 0.26$mm and $e_a = 0.05$mm.

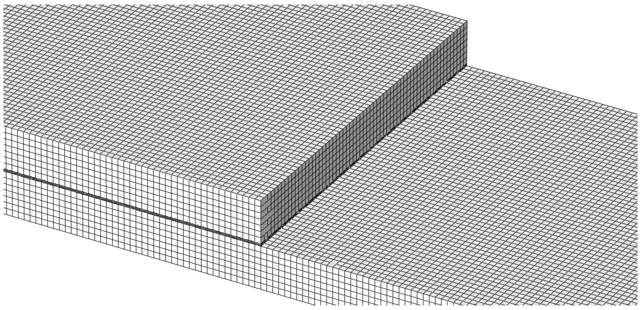

Figure 27: Mesh used in finite element analysis of a single lap adhesive joint

Figure 28 shows the deformation of and stress distribution in the finite element model. This clearly illustrates the bending of the adherends due to the eccentricity of the load path, suggesting that the rigid adherend and Volkersen models (see Section 3.1) significantly oversimplify the mechanics of single lap joints. Notably, the maximum stress in the model is located in the adherend rather than in the adhesive layer.

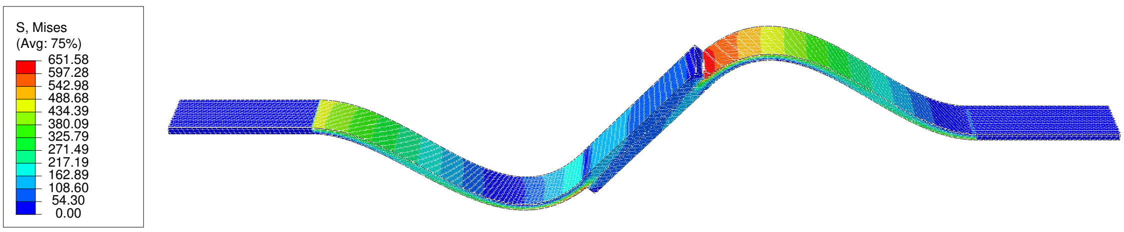

Figure 28: Deformed shape and stress distribution (in MPa)
predicted by finite element analysis of a single lap adhesive joint

In order to compare the predictions of finite element analysis with those of closed-form analysis, the shear stress and peel stress in the adhesive layer were found in elements corresponding the mid-width of the overlap. Figure 29 shows these plotted along with the stress distributions predicted by Goland and Reissner. As with all of the closed-form models discussed, the adherends could only be defined as isotropic. Therefore, two versions of the Goland and Reissner predictions were plotted – one using $E = E_{11} = 48.8$GPa, and one using $E = E_{33} = 2.4$GPa (both from Table 12). The closed-form model also required an input value for the tensile force applied. This was found by inspecting the finite element model.

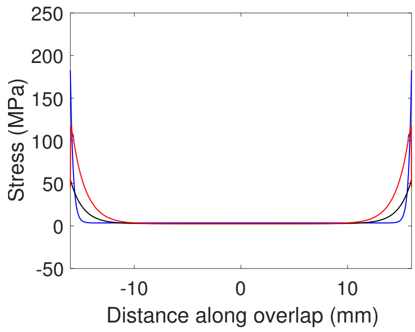

(a) Shear

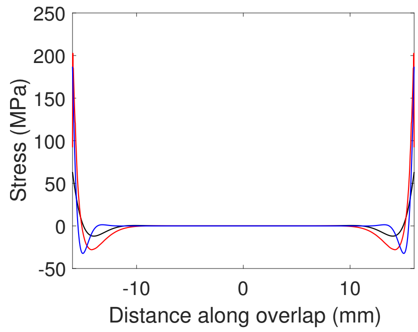

(b) Peel

Figure 29: Adhesive stress distributions predicted by the Goland and Reissner model with $E = 48.8$GPa (black) and $E = 2.4$GPa (blue), and by finite element analysis (red)

It can be seen in Figure 29 that the shapes of the adhesive stress distributions predicted by closed-form analysis approximately match those of finite element analysis. The magnitudes of shear and peel stress are near-zero in the central region of the joint overlap ($-10 \le L \le 10$), and rise to maxima in the end regions. This contrasts with the uniform stress distribution predicted by the rigid adherend analysis (see Figure 15).

Table 13 summarises the maximum stress predictions (to two significant figures) of the closed-form solutions and finite element analysis. This shows significant difference in the closed-form predictions depending on the value used for the adherend elastic modulus (E). When the longitudinal elastic modulus of the composite laminate ($E = 48.8$GPa) was used, the maximum stress predictions were approximately three times smaller than when the through-thickness modulus ($E = 2.4$GPa) was used.

Analytical method	τ_{max}	σ_{max}
Closed-form ($E = 48.8$GPa)	55	63
Closed-form ($E = 2.4$GPa)	180	190
Finite element	120	200

Table 13: Predictions (in MPa) of maximum adhesive shear stress (τ_{max}) and peel stress (σ_{max}) by closed-form analysis and finite element analysis

Both closed-form solutions deviated significantly (by 50-55%) from the finite element solution for the maximum shear stress. One closed-form solution (using $E = 2.4$GPa) was in good agreement with the finite element solution for maximum peel stress (5% difference), while the other (using $E = 48.8$GPa) was not (69% difference). It can be concluded that closed-form analysis using the through-thickness modulus of the laminate results in better agreement with finite element analysis.

3.3 Parametric study [FBS]

One of the advantages of closed-form analysis is that it enables straightforward investigations into the effects of varying parameter values. Even with fixed adhesive and adherend material properties, a great degree of variation in joint strength can be produced by changing a few key geometric parameters – overlap length (L), overlap width (w), adherend thickness (t), and adhesive thickness (t_a).

In order to predict the strength of a joint, failure must be defined. As shown in Figure 30, the number of possible failure modes is greater for joints with fibre-reinforced plastic adherends than for those with ductile metal adherends [48]. The low through-thickness strength of laminates introduces the potential for interlaminar failure. Additionally, transverse failure is common in unidirectional laminate adherends due to Poisson's ratio effects and low transverse strength.

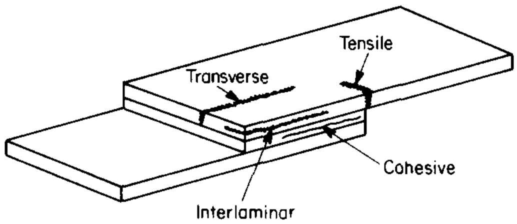

Figure 30: Failure modes in adhesive joints with laminate adherends (from [48])

Simple, stress-based failure criteria were used. Tensile failure in the adherends was defined as

$$\frac{F}{wt} \geq \sigma_{lam} \tag{37}$$

where F is the tensile load, w is the adherend width, t is the adherend thickness, and σ_{lam} is the longitudinal tensile strength of the laminate. Interlaminar failure was assumed to occur when the maximum bending stress (σ_b) in the laminate exceeds the through-thickness strength of the laminate (σ'_{lam}). From elasticity theory, σ_b is given by [14]

$$\sigma_b = \frac{6M}{wt^2} \tag{38}$$

Goland and Reissner's expression for the bending moment (M) on the joint (see Equation 30) can be used to state the interlaminar failure criterion in terms of the tensile load:

$$\sigma_b = \frac{3kF}{wt} \geq \sigma'_{lam} \tag{39}$$

where k is Goland and Reissner's bending moment factor. While common in unidirectional laminates, transverse failure is likely to occur infrequently in the quasi-isotropic laminates used in this project. Therefore, a transverse failure criterion was not defined.

With satisfactory quality control, any non-adherend failure should occur within the adhesive layer (cohesive failure) rather than at the adherend-adhesive interface [48, 69].

Failure in the adhesive layer was defined as the point at which the shear stress (τ) or peel stress (σ) – as predicted by the rigid adherend model, Volkersen model, Goland and Reissner model, and Allman model – exceeds the adhesive shear strength (τ_a) or tensile strength (σ_a) respectively [44]:

$$\tau \geq \tau_a \qquad \text{or} \qquad \sigma \geq \sigma_a \tag{40}$$

Using ranges of geometric parameter values as inputs, a MATLAB program was written to identify the tensile load at which an adhesive joint would be expected to fail. Starting with a low tensile load, the criteria stated above were used to check for failure. The tensile load was repeatedly increased until the criterion of interest was met, thus identifying the predicted failure load of the joint configuration. Only one parameter was varied at once. The default values of all parameters are given in Table 14.

L	w	t	t_a	E	ν	σ_{lam}	σ'_{lam}	E_a	G_a	τ_a	σ_a
32	32	1.9	0.1	2400	0.3	450	90	2400	860	49	67

Table 14: Default geometric parameter values (in mm) and material properties (moduli and strengths in MPa) used in the parametric study

Also given in Table 14 are the material properties used. The adhesive strength values were sourced from da Silva et al's review [44]. The longitudinal strength of the laminates was taken from the experimental results presented in Section 2.2, while the through-thickness strength – assumed to be matrix-dominated [14] – was assigned a value based on the typical tensile strength of epoxy resin [12]. The remaining values were selected on the basis of continuity with Section 3.2.

Figure 31 shows how joint strength is expected to vary with joint parameters when failure is predicted by cohesive failure or adherend failure. All of the models predict a linear increase in joint strength with increasing overlap width. This can be explained with reference to Equations 28-34 and Equation 39: in all cases, the stress predictions are inversely proportional to the joint width. The rigid adherend model also predicts a linear relationship between joint strength and overlap length. However, the other models suggest diminishing strength gains as overlap length is increased. A similar trend is predicted by these models as adherend thickness is increased, while the rigid adherend model predicts no change.

Perhaps the most interesting of the plots is Figure 31d. Two of the models predict that failure load is independent of adhesive thickness. The Volkersen and Goland and Reissner models predict a continuous increase in joint strength as adhesive thickness is increased. In contrast, the Allman model suggests (in agreement with the results of da Silva et al's parametric study [67]) that there is a low adhesive thickness (< 1mm) at which the failure load is a maximum.

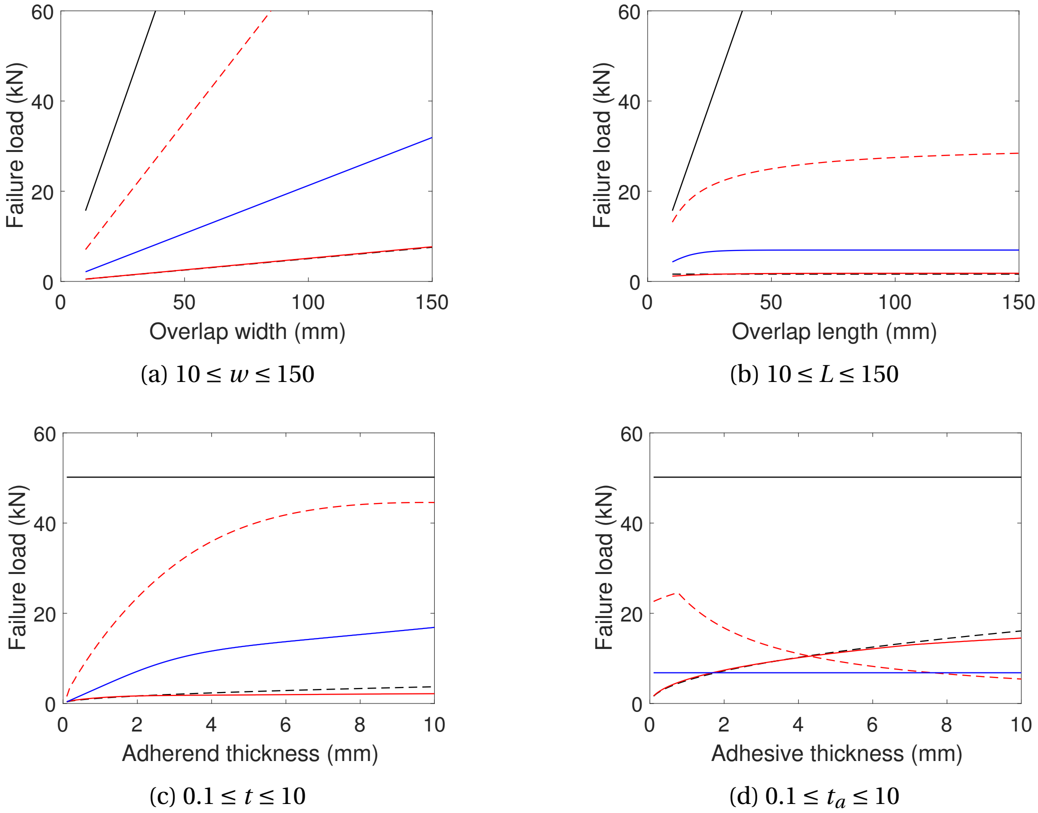

(a) $10 \leq w \leq 150$ (b) $10 \leq L \leq 150$

(c) $0.1 \leq t \leq 10$ (d) $0.1 \leq t_a \leq 10$

Figure 31: Change in failure load with varying geometric parameter values (in mm) as predicted by cohesive failure (rigid adherend model – solid black; Volkersen model – dashed black; Goland and Reissner model – solid red; Allman model – dashed red) and adherend failure (tensile or interlaminar – solid blue)

3.4 Experimental analysis [FBS]

Mechanical tests of adhesive single lap joints were carried out according to ASTM D5868 [56]. Bonded assemblies with carbon-epoxy laminate adherends were mounted in a universal testing machine and statically loaded in tension.

Two sets of tests were carried out. In the first, three adhesives were compared with respect to joint strength. In the second, further investigation was made into the performance of one of the adhesives with thinner adherends.

3.4.1 Adhesive selection [FBS]

In order to identify a set of candidate adhesives that could be used to join fibre-reinforced plastics, a review of literature on adhesive bonding [2, 11, 16, 58, 59, 60] was conducted. Ten families of adhesives were found to be applicable: acrylics, bismaleimides, cyanoacrylates, epoxies, methacrylates, phenolics, polyimides, polyurethanes, silicones, and thermoplastics. These candidates were compared with respect to criteria including availability in the United Kingdom, price per unit volume of adhesive, shear and peel strength, service temperature, water and chemical resistance, product form, and cure conditions. This is a subset of the criteria described in Section 6.3, and is comparable to the set of adhesive selection factors found in the European Space Agency's adhesive bonding handbook [57].

Table 33 in Appendix A was used to compare the adhesives. In cases where all candidates were found to be the same with respect to a certain criterion, or where there was insufficient information on which to base a decision, the criterion was not included in the comparison table. For example, the service temperature ranges of all the adhesives were found to extend beyond what could be expected in operation in the United Kingdom [61]. Hence, comparing the adhesives with respect to their minimum and maximum service temperatures was decided not be valuable in the selection process.

A screening process was carried out with a generic set of design requirements that could be expected in Formula Student:

> **Suitability for structural applications (shear strength > 7MPa):** reject silicones, thermoplastics
>
> **Ability to cure at room temperature:** reject bismaleimides, phenolics, polyimides
>
> **Good water and chemical resistance:** reject cyanoacrylates
>
> **Low cost (price < £30/100ml):** reject acrylics

The quantitative shear strength limit was set in accordance with European Space Agency guidance [57]. The requirement for room temperature curing was based on a consideration of manufacturability: for all but the smallest assemblies, curing the adhesive at elevated temperatures could be impracticable. Using an adhesive that degrades significantly when wet was judged to be a significant deficiency in the context of Formula Student. Finally, affordability was considered by setting a limit on the price of the adhesive. Following this screening process, the remaining candidates were epoxies, methacrylates and polyurethanes.

3.4.2 Specimens and method [FBS]

Figure 32 shows a schematic of the specimens used to test the adhesives. As in the tests described in Section 2.2, protective fibreglass tabs were bonded to the non-overlapping ends of the laminate using epoxy adhesive. The nominal dimensions of the specimen are given in Table 15.

It is recommended in ASTM D5868 that laminates with a thickness of 2.5mm be used for testing adhesives [56]. Therefore, the 3mm nominal thickness laminate (mean actual thickness of $t = 2.7$mm) was used for the first set of tests, in which three types of adhesive were compared. In the second set of tests, one of the adhesives was investigated further using 2mm nominal thickness laminate (mean actual thickness of $t = 1.9$mm).

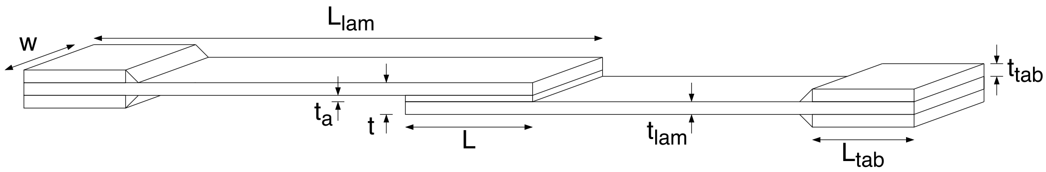

Figure 32: Specimen geometry used in mechanical tests of adhesive joints

Epoxy (Permabond ET500 [62]), methacrylate (VuduGlu VM100 Black [63]) and polyurethane (Permabond PT326 [64]) adhesives were procured. A set of five specimens was manufactured with each adhesive. The specimens were made by following a process similar to that described in Section 2.2. The key additional source of manufacturing variability was the process of joining the two adherends.

w	L	t_a	L_{lam}	t_{lam}	L_{tab}	t_{tab}
32	32	0.1	145	3	0.3	2

Table 15: Nominal dimensions (in mm) of the adhesive joint specimens

Three critical dimensions of the joints were measured using vernier calipers. The width (w) and length (L) of the overlap were used to determine the bond area, while the thickness (t) of the overlap was used to estimate the bond thickness. Table 16 presents a summary of these measurements for the set of specimens made with 3mm nominal thickness laminate. Mean ($\bar{x}$) and standard deviation (s) values are quoted to the resolution of the calipers used (0.01mm).

Adhesive type	w	L	t
Epoxy	32.53 ± 0.52	32.31 ± 0.76	5.40 ± 0.05
Methacrylate	32.20 ± 0.16	32.59 ± 0.55	5.42 ± 0.08
Polyurethane	32.41 ± 0.18	32.60 ± 0.23	5.50 ± 0.16

Table 16: Measurements ($\bar{x} \pm s$ in mm) of critical dimensions of adhesive joint specimens with $t_{lam} = 3$mm

In the second set of tests, laminate of nominal thickness $t_{lam} = 2$mm was used. All other nominal dimensions were the same as before. Table 17 presents the mean and standard deviation values of the actual dimensions.

Adhesive type	w	L	t
Methacrylate	32.35 ± 0.19	32.59 ± 0.66	3.82 ± 0.01

Table 17: Measurements ($\bar{x} \pm s$ in mm) of critical dimensions of adhesive joint specimens with $t_{lam} = 2$mm

Each specimen was mounted in a universal testing machine with its ends clamped by hydraulic grips, which applied a pressure of 20MPa. In order to achieve correct alignment in the grips of the machine, steel spacers were used, and an engineer's square was used for visual checks. The grips were separated longitudinally at a cross-head speed of 12.7mm/min. The tensile force in the specimen was measured using an 80kN load cell. A clip-on extensometer was used to measure the longitudinal extension of the central region of the specimen. The distance between the extensometer arms before loading was $L_0 = 50$mm.

3.4.3 Results [FBS]

The average adhesive shear stress (τ_0) was calculated by normalising the tensile force with respect to the bond area (see Equation 28), thus accounting for manufacturing variations. The longitudinal strain of the joint (ϵ) was calculated by finding the change in distance (Δ) between the extensometer arms, and normalising with respect to the distance before loading (L_0), as in Equation 18. Figures 33a-33c show plots of τ_0 against ϵ for the specimens made with 3mm laminates. Table 18 presents sample mean ($\bar{x}$) and standard deviation (s) values for failure stress (τ_f) and failure strain (ϵ_f), calculated according to Equations 21 and 22.

Adhesive type	**τ_f (MPa)**	**ϵ_f (%)**
Epoxy	12.90 ± 2.16	0.89 ± 0.09
Methacrylate	13.39 ± 1.50	0.33 ± 0.04
Polyurethane	13.32 ± 0.86	0.35 ± 0.05

Table 18: Experimentally determined failure stress and strain ($\bar{x} \pm s$) of adhesive joint specimens with $t_{lam} = 3$mm

As described in Section 3.4, the statistical significance of the results was tested using the Peirce criterion. One methacrylate specimen and two polyurethane specimens were found to produce outlying results. After eliminating the outliers, the sample mean and standard deviation were recalculated. These adjusted values are presented in Table 19 and Figure 33d.

Adhesive type	**τ_f (MPa)**	**ϵ_f (%)**
Epoxy	12.90 ± 2.16	0.89 ± 0.09
Methacrylate	14.04 ± 0.43	0.34 ± 0.03
Polyurethane	13.82 ± 0.44	0.36 ± 0.03

Table 19: Experimentally determined failure stress and strain ($\bar{x} \pm s$) of adhesive joint specimens with $t_{lam} = 3$mm after eliminating outliers

Based on the failure stress results, the methacrylate adhesive was selected for further

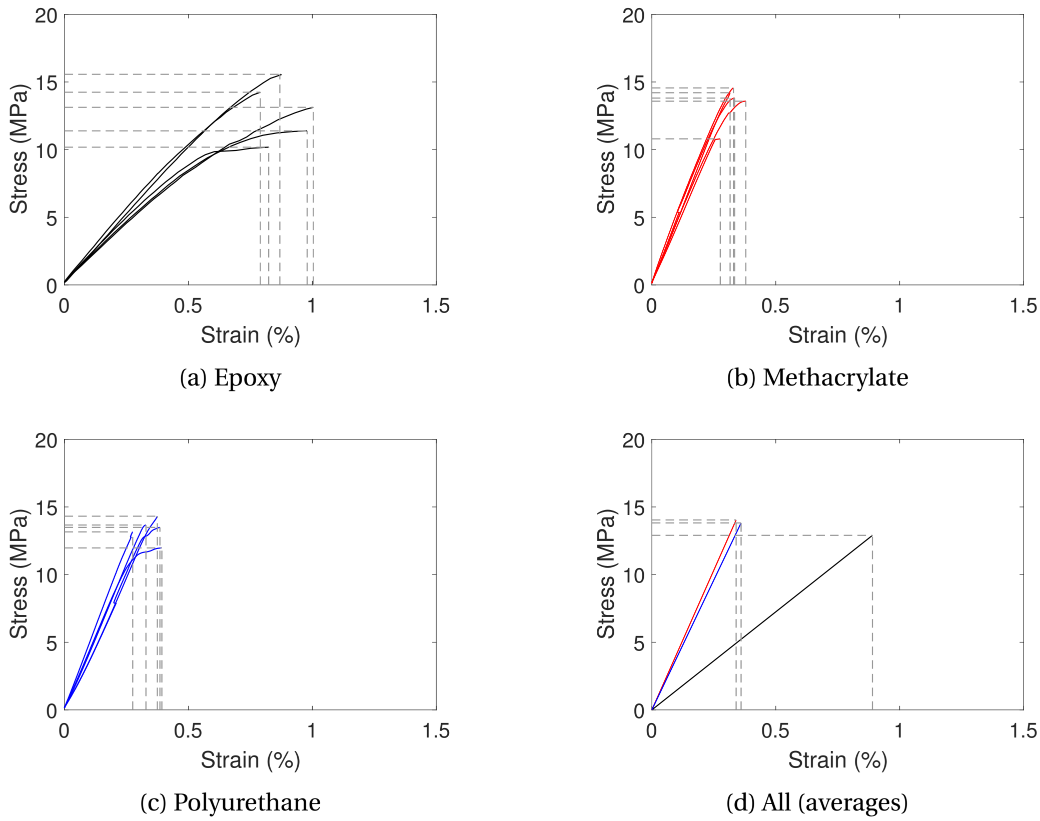

(a) Epoxy (b) Methacrylate

(c) Polyurethane (d) All (averages)

Figure 33: Experimentally determined longitudinal stress-strain responses of single lap joints (t_{lam} = 3mm) made with epoxy (black), methacrylate (red), and polyurethane (blue) adhesives

investigation in the second set of tests. Figure 34a shows plots of the average shear stress in the adhesive (τ_0) against the longitudinal strain of the joint (ϵ).

One outlier was identified. The sample mean and standard deviation values for failure stress (τ_f) and failure strain (ϵ_f) – re-calculated after eliminating this outlier – are given in Table 20.

Adhesive type	τ_f **(MPa)**	ϵ_f **(%)**
Methacrylate	11.17 ± 0.82	0.79 ± 0.05

Table 20: Experimentally determined failure stress and strain ($\bar{x} \pm s$) of adhesive joint specimens with t_{lam} = 2mm after eliminating outliers

Figure 34b shows a comparison of the average stress-strain curves for the methacrylate joints made with laminates of different thicknesses.

3.5 Discussion [FBS]

The predictions of the theoretical analyses are compared with each other, and then with the experimental results. The merits and limitations of each analysis are discussed.

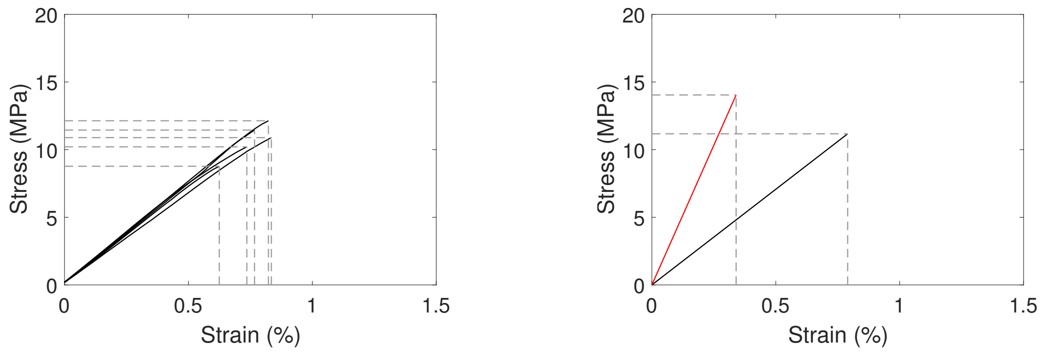

(a) 2mm-thick adherends

(b) 2mm- and 3mm-thick adherends

Figure 34: Experimentally determined longitudinal stress-strain responses of methacrylate adhesive joints with $t_{lam} = 2$mm (black) and $t_{lam} = 3$mm (red)

3.5.1 Comparison of strength predictions with results [FBS]

The programs used for the parametric study (Section 3.3) were to predict the failure load of the joints tested experimentally. Geometric parameters were assigned values corresponding to the mean measured dimensions of the test specimens. Adhesive material properties were sourced from manufacturers' data sheets [62, 63, 64] where possible, and from materials databases [65] for the remaining information. Table 21 presents (to two significant figures) the failure load (F_f) predicted by the closed-form models in comparison with the experimental results.

Adhesive type	F_{fR}	F_{fV}	F_{fGR}	F_{fA}	F_{fLAM}	F_{fEX}
Epoxy	22	0.3	0.2	12	9.3	13.6
Methacrylate	40	1.2	1.0	18	9.3	15.0
Polyurethane	12	1.4	1.2	6	9.3	14.7
Methacrylate (2mm)	40	0.7	0.7	15	6.9	12.6

Table 21: Failure load (in kN) predicted by a cohesive failure criterion (rigid adherend model – F_{fR}; Volkersen model – F_{fV}; Goland and Reissner model – F_{fGR}; Allman model – F_{fA}), and by an adherend failure criterion (F_{fLAM}); mean failure load (in kN) from experimental results (F_{fEX})

It is clear from Table 21 that the Volkersen and Goland and Reissner models significantly underestimate (by up to two orders of magnitude) the strength of real adhesive joints. Across all sets of adhesive joint tests, the predictions of both of these models were found to have root-mean-square (RMS) deviation of approximately 13kN from the experimental results. This can be understood with reference to Figure 17. Both models predict very high stresses at the ends of the overlap, so the failure criterion is met at relatively low tensile loads.

In contrast, the rigid adherend model tends to overestimate joint strength (RMS deviation of 19kN from results) because it predicts relatively low shear stress and zero peel stress. Of all the failure prediction methods, finding the load for cohesive failure according to

Allman's model provides the most consistent accuracy to the experimental results (RMS deviation of 4.8kN).

Given the simplicity of the adherend failure criterion, it predicted the results with good accuracy (RMS deviation of 5.3kN). The fact that nearly 80% of specimens failed in the adherends suggests that developments to this failure criterion would be valuable for strength prediction.

Aside from the theoretical inaccuracies of the closed-form models (see Section 3.5.2), a fundamental limitation on the utility of these predictions was the accuracy of the input values used. As discussed in Section 3.5.4, the information provided by manufacturers is rarely sufficient for adequately defining materials in theoretical analysis. With better knowledge of the adhesives and adherends, the theoretical predictions could be expected to agree better with experimental results.

3.5.2 Evaluation of closed-form analysis [FBS]

The closed-form models discussed in Section 3.1 are valuable for understanding the physical phenomena that affect joint behaviour. As more physical effects are incorporated into the solutions, the stress predictions change in ways that make intuitive sense.

This analytical approach also facilitates relatively fast estimation of the stress state in a joint (not necessarily requiring a computer). By extension, it allows parametric studies to be carried out quickly and without extensive additional work.

However, the models used for this work highlight an important limitation of closed-form solutions. The simplifications made to produce manageable mathematical expressions also reduce the accuracy with which physical effects in real joints are modelled [48].

Some of these simplifications are more acceptable than others. As shown by Adams and Peppiatt's analysis, the stresses in the width direction of the joint are relatively small. Therefore, two-dimensional models of joints are generally sufficient [40].

The experimental results shown in Figures 33 and 34 suggest that the assumption of linear elastic adhesive behaviour is not completely valid, perhaps most clearly in the case of the epoxy specimens. However, the plastic strain observed was small relative to the elastic region, and it can be concluded that the adhesives were sufficiently linear elastic and brittle to justify this assumption [40].

Where the closed-form analyses fall notably short is in their treatment of the adherends. The elastic properties can only be defined with two parameters (elastic modulus and Poisson's ratio), thus requiring an assumption of isotropic behaviour. Thus, fibre-reinforced plastics cannot be accurately represented.

A further limitation is the inability to account for geometric variations from the idealised single lap joint. As discussed in Section 3.5.5, real joints are not perfectly square at the ends of the overlap, but rather have fillets formed by excess adhesive. The shape and size of these fillets were found by Lang and Mallick [66] to have a significant effect on the strength of joints. Therefore, the closed-form models used are limited in the extent to which they can model joints accurately.

Attempts to provide more general closed-form solutions have resulted in greater complexity in calculation (many models require iterative methods) thus undermining the benefit of closed-form analysis [40]. Therefore, while a great number of extensive analytical models do exist, not all of them can give the straightforward insights provided by the models used for this work.

Future work could be carried out using more developed closed-form models, such as those that account for material nonlinearity. However, it may be more beneficial to focus on refining the finite element analysis carried out.

3.5.3 Evaluation of finite element analysis [FBS]

The finite element model discussed in Section 3.2 addressed some of the shortfalls of the closed-form models. The anisotropic elastic properties of the adherends were fully defined, and three-dimensional physical effects were included. The broad agreement between the closed-form and finite element analyses, combined with the approximate agreement between the theoretical predictions and the experimental results, suggests that the finite element model matched the behaviour of real joints with reasonable accuracy.

Unlike with closed-form solutions, making stress predictions by finite element analysis does not become significantly more labour-intensive as the model is made more complex. For example, material nonlinearity and geometric variations can be incorporated into a finite element model relatively quickly. This allows the scope of analysis to be extended to include almost any physical effects of interest. Indeed, Adams et al [14] argued that finite element techniques are the best tool available for theoretical investigations into the mechanics of real joints.

A number of refinements could be made to the finite element model in order to better reflect the joints tested experimentally. Considering that the maximum stress in the finite element model was found to be in the adherends (see Figure 25), the material implementations could be refined by incorporating plasticity and failure models. The geometry could be made more realistic by including adhesive fillets at the ends of the overlap.

Abaqus offers the option to model adhesive layers with special cohesive elements [68]. An investigation could be made into the effects of using these elements instead of general-purpose continuum elements. A rigorous analysis might consider the effect of residual thermal strains from the adhesive curing process [48]. Finally, Abaqus can be used to conduct parametric studies [68]. Thus, the work described in Section 3.3 could be developed to include the predictions of more comprehensive theoretical models.

3.5.4 Evaluation of adhesive selection process [FBS]

The process of adhesive selection was, in part, limited by the content of the data sheets provided by manufacturers. There was considerable variation in the type and amount of information provided.

The adhesive strength values presented in the data sheets were not all determined using the same test method or specimens. As noted by Hart-Smith [51], the adherends have a significant influence on the results obtained in single lap shear tests. The data generated when using, for example, steel adherends cannot accurately be used to predict the shear strength of the same adhesive with composite adherends.

Further problems were introduced by qualitative, rather than quantitative, statements of performance with respect to design criteria such as water resistance. Without standardised measurements quoted by all manufacturers, ambiguity was introduced, reducing the utility of comparison using these criteria. Data in greater quantity and of higher quality would have enabled a more informed comparison of the adhesives.

In the absence of a specific design scenario (and, therefore, a well-defined design specification), the adhesive selection process was also somewhat arbitrary. However, the process was judged to be indicative of how a future Formula Student team could identify the adhesives that best suit its design requirements.

3.5.5 Evaluation of experimental analysis [FBS]

As in the tests described in Section 2.2, manufacturing variations occurred when applying the protective end tabs to the laminates, and when cutting the specimens to size. The manufacture of adhesive joints introduced additional sources of inconsistency. First, the overlap and alignment of the adherends relative to each other were liable to variation. Second, the thickness of the adhesive layer was not actively controlled. Third, the shape and size of the 'spew' fillet, formed by the adhesive squeezed out during the clamping of the joint, were variable.

These issues could be addressed with relative ease. The fixture shown in Figure 35, proposed in Broughton and Gower's good practice guide [37], would allow fine control of alignment, overlap, bond thickness and fillet shape. An additional measure to control the geometry of the adhesive layer is incorporating small glass beads or lengths of metal wire as spacers in the bond area, thus ensuring a minimum thickness.

The testing setup used provided enough information to compare the different types of adhesive joints on the basis of failure strength and longitudinal extension. If Poisson's

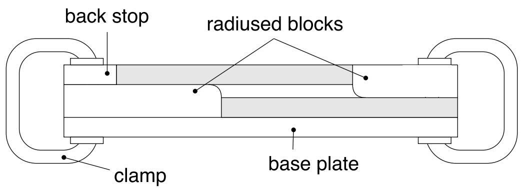

Figure 35: Fixture for controlling the geometry of single lap joint specimens

ratio strains were to be investigated, a video extensometer could be used. This method of measuring the deformation of the specimens has an additional benefit: as a non-contact method, it would not induce or resist deformation in the specimens. For the experiments described in Section 3.4, it was assumed (based on the rigidity of the laminates) that the use of a clip-on extensometer had negligible effects on the results.

4 Mechanical fastening [AV]

In mechanically fastened lap joints between fibre-reinforced plastics, tensile loads in the joined components are transmitted through the fastener, which is loaded in shear. The composite sheets experience a bearing load on the hole through which the fastener passes. When examining this joining method, it is important to consider not only the response of the fibre-reinforced plastic to bearing loads, but also the response of the fastener to shear loads. These two aspects of mechanically fastened joints were investigated both theoretically and experimentally.

The tensile strength of fibre-reinforced plastics comes primarily from the strength of carbon fibres. Drilling a hole in a component of this material results in the cutting of some reinforcing fibres. This introduces a discontinuity in the composite, which can significantly its strength. Therefore, the analysis of mechanically fastened joints is more complex for these materials than for traditional structural alloys. The 2mm-thick laminate discussed in Sections 2-3 was used for investigating mechanical fastening.

4.1 Pin-loaded holes [AV]

A pin-loaded hole in a laminate can fail in one of three common modes – tension failure, shearout failure or bearing failure (see Figure 36).

Tension failure and shearout failure primarily occur in parts with small values of edge distance and width. Therefore, they are not only dependent on the material and thickness of the plate but also on its geometry. On the other hand, bearing failure, for large enough values of edge distance and plate width, is independent of the shape of the plate and thus is applicable to more cases. For this reason, bearing failure is the failure mode of interest. In order to ensure that bearing failure occurs, it is recommended that an edge distance

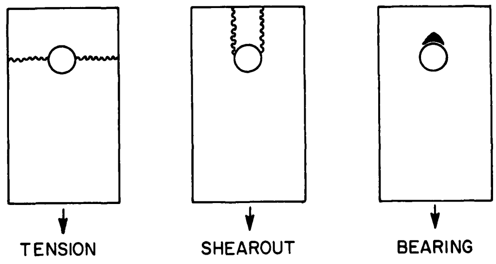

Figure 36: Failure modes of a pin-loaded holes in laminates (from [72])

to hole diameter ratio and a width to hole diameter ratio greater than 2 is used [79].

4.1.1 Theoretical stress analysis [AV]

Consider a pin-loaded hole in a plate. The radial stress distribution in the half of the plate that experiences the force is given by

$$\sigma = \sigma_m \cos(\theta) \tag{41}$$

where σ_m is the maximum stress in the radial direction due to the force on the plate, and θ is the angle measured from the direction that the load is applied [75].

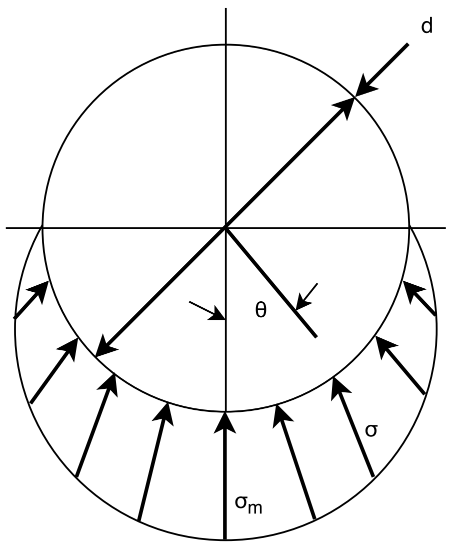

Figure 37: Radial stress distribution around a pin-loaded hole (from [75])

By integrating the stress in the loaded part of the plate with respect to the angle on the half of the plate that is loaded, the tensile force (F) on the hole can be expressed in terms of the maximum bearing stress:

$$F = \frac{\pi}{4}\sigma_m t d \tag{42}$$

where t is the thickness of the plate and d is the diameter of the hole. Assuming that the pin and hole surfaces are smooth and that the clearance between the pin and the hole is minimal, the bearing stress is conventionally given as a uniform stress acting on the projected cross-sectional area of the hole:

$$\sigma = \frac{F}{td} \tag{43}$$

4.1.2 Strength prediction assuming isotropy [AV]

The laminate used for the tests was manufactured using a quasi-isotropic layup and was loaded along its primary (0°) axis. Therefore, in order to find an initial estimate for the load at which the laminates are expected to fail, it was assumed that the composite behaves as an isotropic material. Based on this, bearing failure is expected to occur when the bearing stress exceeds the ultimate tensile strength (σ_u) of the material. Using $\sigma_u = 447.3$MPa from Section 2.2, a laminate thickness of $t = 1.9$mm, and a hole diameter of $d = 6$mm, Equation 43 can be rearranged to predict the failure load (F_{max}):

$$F_{max} = \sigma_u td = 447.3 \times 1.9 \times 6 = 5.1\text{kN} \tag{44}$$

There is a stress concentration factor (k_s) at the edge of a pin-loaded hole in a plate. Chang et al [72] found that applying a stress concentration factor results in a more accurate estimate for the load at which bearing failure occurs. Based on their findings for plates of similar hole diameter to width ratios, a value of $k_s = 0.985$ was used. Thus, the adjusted failure load is

$$F'_{max} = \frac{F_{max}}{k_s} = \frac{5.1}{0.985} = 5.2\text{kN} \tag{45}$$

4.1.3 Strength prediction including anisotropy [AV]

Analytical techniques for estimating the bearing strength of laminates were investigated in order to find a more accurate estimate that accounts for the anisotropy of the material. These techniques are semi-empirical in that they require the properties of the individual plies that make up the laminate in order to make a strength prediction. Unless the manufacturer of the material provides all of the lamina properties, which is seldom the case, they need to be found experimentally.

The Yamada failure criterion [71] was used in an attempt to estimate the load at which failure would occur. This criterion considers the laminate to have failed when the final lamina fails. This occurs when the following relationship is satisfied:

$$\left(\frac{\sigma_1}{X}\right)^2 + \left(\frac{\tau_{12}}{S_c}\right)^2 \geq 1 \tag{46}$$

where σ_1 is the longitudinal stress, τ_{12} is the shear stress in each ply, X is the ply longitudinal strength and S_c is the ply shear strength of a symmetric cross ply laminate (a laminate whose layup is symmetric about its neutral axis and in perpendicular pairs).

A MATLAB implementation of Yamada's analytical solution was written to investigate the laminate used for testing. The failure load was found to be F_{max} = 3.2kN. However, Yamada noted that the laminate shear strength has been found to be approximately three times greater than the shear strength of individual plies. Accounting for this in the calculations resulted in an adjusted failure load prediction of F'_{max} = 5.0kN.

4.1.4 Experimental analysis [AV]

Mechanical tests of drilled laminates were carried out according to ASTM D5961 [90]. Specimens were mounted in a universal testing machine and statically loaded in tension by a smooth bolt through a hole on the centreline of specimen.

Specimens and method [AV]

Figure 38 shows a schematic of the specimens used to investigate the bearing response of the laminates. As in the tests described in Sections 2.2 and 3.4, protective tabs were bonded to the gripped ends of the laminate. The nominal dimensions of the specimen are given in Table 22.

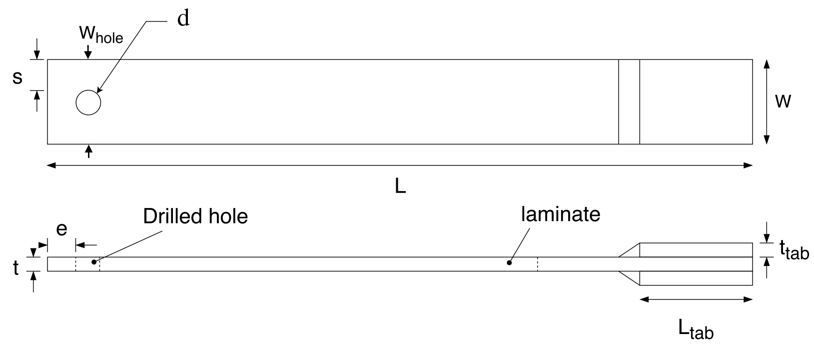

Figure 38: Specimen geometry used in mechanical tests of pin-loaded holes

The specimens were manufactured by following a process similar to that described in Section 2.2. The key additional step was drilling a hole in the laminate. The material was clamped between two 2mm-thick sheets of acrylic to minimise the risk of delamination damage at the edges of the hole. A specialist carbide drill bit with a sickle point was used. This drill bit is designed to cut at the edge of the hole first in order to cut the individual fibres rather than force them out of the way.

In order to quantify variations that occurred during manufacture, five dimensions of each specimen were measured using vernier calipers. Table 23 presents a summary of the measurements, stating mean ($\bar{x}$) and standard deviation (s) values to the resolution of the calipers used (0.01mm).

w	L	t	e	s	d	L_{tab}	t_{tab}
32	145	1.9	16	16	6	40	2

Table 22: Nominal dimensions (in mm) of the pin-loaded hole specimens

Five specimens were tested. The tabbed end of each specimen was clamped in the grips of the testing machine. The other end of the specimen was mounted in the assembly illustrated in Figure 39, which was clamped in the second pair of machine grips.

w	L	e	s	d
32.05 ± 0.08	145.52 ± 0.31	15.94 ± 0.36	15.54 ± 0.29	6.02 ± 0.01

Table 23: Measured dimensions ($\bar{x} \pm s$ in mm) of the pin-loaded hole specimens

Although its end region was threaded, the bolt was smooth in the region in contact with the specimen. The nut was tightened to the point were it just made contact with the metal plate so that the clamping force on the specimen was minimal. An engineer's square was used to for visual checks of specimen alignment. The grips were separated longitudinally at a rate of 2mm/min. The tensile force was measured using a 100kN load cell.

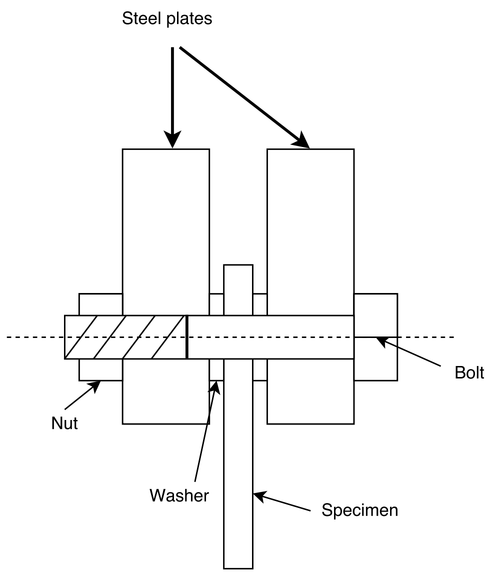

Figure 39: Assembly used in mechanical tests of pin-loaded holes

Results [AV]

Figure 40 shows the variation in measured tensile load with increasing grip separation.

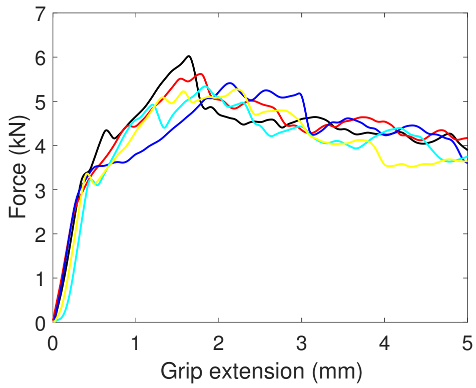

Figure 40: Experimentally determined longitudinal tensile force-extension responses of pin-loaded holes

The maximum load in each data set was found. In addition, the elastic limit was identified. In order to achieve this, the gradient in a linear range (grip extension up to 0.4mm by visual inspection) was calculated. The elastic limit was then defined as the point at which the gradient of the force-extension curve changes by more than 100% of the linear gradient.

Applying the Peirce criterion as described in Section 2.2 revealed that one specimen produced results that did not conform with the rest. After eliminating the outlier, the sample mean ($\bar{x}$) and standard deviation (s) were calculated for load and extension at the elastic limit (F_e and X_e respectively), and for maximum load (F_{max}) and corresponding extension (X_{Fmax}). These are presented in Table 24.

F_e (kN)	X_e (mm)	F_{max} (kN)	X_{Fmax} (mm)
3.16 ± 0.06	0.47 ± 0.06	5.41 ± 0.13	1.99 ± 0.19

Table 24: Experimentally determined tensile load and machine grip extension ($\bar{x} \pm s$) at the elastic limit and at the point of maximum load of pin-loaded hole specimens

4.1.5 Discussion [AV]

The predictions of theoretical analysis are compared with the experimental results. An attempt is made to identify sources of inaccuracy in the theoretical models and variation in experimental testing. A conclusion is drawn as to the value and validity of the results produced by both methods of analysis.

Comparison of predictions to results [AV]

The unsteady force-extension plots in Figure 40 contrast with the smooth plots that would be expected with ductile metal specimens. There were sudden dips in the load with increasing extension. It was observed that cracking noises were audible at instances when the load reading changed suddenly. The unsteady bearing response of the laminate can be explained physically: some fibres break while the matrix and other fibres remain intact.

The failure load determined theoretically using an isotropic assumption was only 4% lower than the mean value determined experimentally. This suggests that this simple model might be sufficient for predicting the failure load of pin-loaded holes in quasi-isotropic laminates. The prediction made using the Yamada failure criterion was more conservative, estimating a failure load 7% smaller than the average experimental value. This inaccuracy is most likely due to Yamada's criterion not accounting for woven laminae and thus neglecting the transverse stiffness of each lamina. Based on the generally good agreement between the theoretical predictions and the experimental results, it can be concluded that the data produced were valid.

It is also important to note the way in which the laminate failed during the experiment. Some fibres had already failed by the time the maximum load was reached. Thus, the specimen had been permanently damaged. It can be seen in Figure 40 that the first dip in the force value occurs at around 3.2kN which suggests that this is the point where the first fibres begin to fail. Therefore, this does appear to be the point were permanent damage to the laminate occurs and it could be best when designing a joint to use this as a loading limit.

Outliers [AV]

The existence of an outlier in the experimental results could be due to variations in the process of manufacturing the specimens. The specimens were slightly longer than the intended length due to excess glue that squeezed out from between the tabs and the laminate during curing. On average, the width of the specimens, measured along the centreline of the hole, was slightly greater than intended. However, the variations in the overall length and width of the specimens should not have significantly affected the results.

Inconsistency in the position and diameter of the hole could have been critical. All hole diameters were within 0.01mm of the nominal dimension. While this level of variation is small, it might have led to non-trivial differences in the tightness of the fit between the bolt and the hole in each specimen, introducing an additional stress concentration factor. Similarly, variations in the distance of the centre of the hole from the edges of the specimen could introduce an 'edge effect' which would also behave as a stress concentrator on the material around the loaded portion of the hole. Finally, there may have been inconsistency in the torque applied to the nut as it was tightened. The nut on the outlying specimen might have been tightened more than on the other specimens, causing a greater clamping pressure to be exerted on the specimen. This could account for the greater-than-expected failing load.

Future work [AV]

Collings [73] proposed a semi-empirical method for predicting the bearing strength of a laminate, and found it to be very accurate. However, in order to estimate the bearing strength of a full laminate, mechanical tests must be carried out on all of the individual plies to determine their bearing strength. The advantage of Collings' method is that, once the required properties are known for all the individual plies that are to be used, different layup sequences can be modelled. Therefore, the layup sequence for the composite that will yield the highest bearing strength can be determined.

Collings' method has drawbacks. It only deals with laminates made up of unidirectional plies oriented at $0°$, $\pm 45°$ and $90°$, thus not accounting for woven plies. It is time- and resource-intensive due to the experiments required on the individual plies. Nevertheless, it could be a useful tool for the Formula Student team to use in the future with the purpose of determining the optimal layup sequence for the composite parts of the vehicle that are going to experience a bearing load.

4.2 Bolted joints [AV]

In bolted lap joints, some of the load is not transmitted as a shear load in the fastener, but instead by solid friction between the two samples. This frictional force (S) results from the clamping force (F_{pre}) exerted by the bolt on the two samples. Up to the value of the frictional force, the entirety of the load through the joint is transmitted through friction. Only for loads greater than this will bearing loads exist. It is assumed that the load transmitted by friction will not affect the bearing load and vice versa. Therefore, the overall load on the joint when bearing failure occurs will be the sum of the bearing load and the frictional load.

In the assemblies used to investigate bolted joints, the bolts were tightened to 2.2Nm using a torque wrench. The preload (clamping force) is given by

$$F_{pre} = \frac{T}{KD} \tag{47}$$

where T is the torque applied to the bolt, K is the nut factor and D is the nominal diameter of the bolt. For metric fasteners, the nut factor is approximately 0.2 [53]. The force transmitted through friction is given by

$$S = \mu F_{pre} \tag{48}$$

where μ is the coefficient of friction between two sheets of composite, which was found in the literature to be approximately 0.74 for worn surfaces [70]. The specimens used for the tests were grit-blasted in order to roughen the surface and simulate a worn surface. This was done to eliminate discrepancies between the samples due to surface variations and thus ensure consistent surface roughness for all samples. It was assumed that the surfaces of the specimens would behave as if they were worn. Therefore, the estimated load transmitted through friction is $S = 1.393$kN, and the predicted overall strength of the joint is $F = 6.7$kN (based on the bearing failure load calculated in Section 4.1.1).

4.2.1 Experimental analysis [AV]

Mechanical tests of bolted single lap joints were carried out according to ASTM D5961 [90]. Specimens were mounted in a universal testing machine and statically loaded in tension.

Specimens and method [AV]

For each specimen (see Figure 41, two laminate pieces with the same geometry as shown in Figure 38 were assembled in a single lap joint configuration using an M6x30mm cap head bolt with a nut. The bolt was tightened to 2.2Nm using a torque wrench. The laminate pieces were manufactured in the same way as those used for the bearing response test.

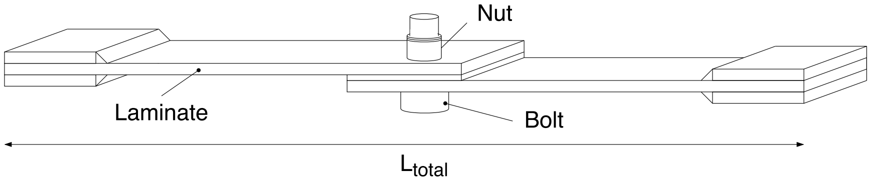

Figure 41: Specimen geometry used in mechanical tests of bolted joints

The laminate pieces were manufactured with the nominal dimensions stated in Table 22. Measurements were taken to quantify manufacturing variations. These are summarised in Table 25, which presents mean ($\bar{x}$) and standard deviation (s) values to the resolution of the calipers used (0.01mm).

w	L	e	s	d
32.10 ± 0.14	145.46 ± 0.63	16.12 ± 0.29	15.86 ± 0.15	6.00 ± 0.00

Table 25: Measured dimensions ($\bar{x} \pm s$ in mm) of bolted joint specimens

Five specimens were made, but one was damaged in handling. Therefore, four specimens were tested. Each specimen was mounted in a universal testing machine with its ends clamped by hydraulic grips. Steel spacers were used to align the joint assembly with the loading axis of the machine. An engineer's square was used for visual checks of alignment. The machine grips were separately longitudinally at a cross-head speed of 2mm/min. The tensile force in the specimen was measured using an 80kN load cell. A clip-on extensometer was used to measure the longitudinal extension of the central region of the specimen. The distance between the extensometer arms before loading was $L_0 = 50$mm. The extensometer was removed just before its maximum range of 5mm extension was hit. The tests were then continued until after a clear maximum load was reached.

Results [AV]

Figure 42a shows the variation in measured tensile load with increasing grip separation. Figure 42b shows a similar plot, but with extension measured by the clip-on extensometer up to its maximum extension.

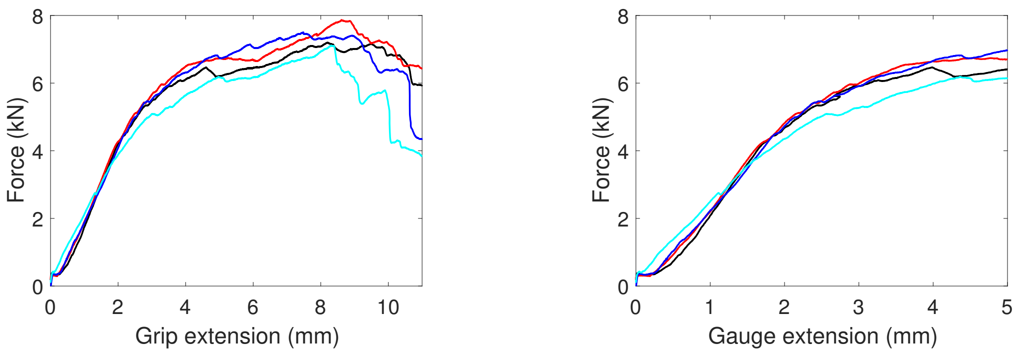

(a) Machine grip extension (b) Clip-on extensometer extension

Figure 42: Experimentally determined longitudinal tensile force-extension responses of bolted joints

The maximum load in each data set was found. In addition, the elastic limit was identified. In order to achieve this, the gradient in a linear range (grip extension of 0.5-1.5mm by visual inspection) was calculated. The elastic limit was then defined as the point at which the gradient of the force-extension curve changes by more than 20% of the linear gradient.

Applying the Peirce criterion as described in Section 2.2 revealed that one specimen produced results that did not conform with the rest. After eliminating the outlier, the sample mean ($\bar{x}$) and standard deviation (s) were calculated for load and extension at the elastic limit (F_e and X_e respectively), and for maximum load (F_{max}) and corresponding extension (X_{Fmax}). These are presented in Table 26.

F_e (kN)	X_e (mm)	F_{max} (kN)	X_{Fmax} (mm)
4.23 ± 0.16	2.08 ± 0.03	7.27 ± 0.17	8.00 ± 0.37

Table 26: Experimentally determined tensile load and machine grip extension ($\bar{x} \pm s$) at the elastic limit and at the point of maximum load of bolted joint specimens

4.2.2 Discussion [AV]

The experimentally determined maximum load of 7.3kN exceeded the predicted value of 6.7kN. This difference has multiple possible explanations. First, using a torque wrench on unlubricated bolts to control the preload on the joint has a range of accuracy of ±35% of the applied preload [76]. Taking this into account means that the maximum expected load could vary between 6.2kN and 7.2kN. Second, the region of the bolt shaft in contact with the hole in the laminate was threaded (compared with a smooth surface in the bearing response tests). The load being exerted on the hole by the threaded surface instead of a smooth surface will have affected the stress distribution in the material and hence the maximum load that could be supported by the joint.

It has been shown that the bearing strength of laminates increases significantly when they are (even lightly) clamped. This is because the plies are pressed together and delamination of the plies is resisted [78]. The clamping force on the joint in this test was not present in the bearing response test. This might explain why the laminate did not reach as high a load during the bearing response experiment. Clamping may also explain the greater smoothness of the plots shown in Figure 42 (bolted joint) compared with those in Figure 40 (bearing response). In the bolted joints, due to the greater through-thickness compressive force, the failure of individual fibres would have had a smaller effect on the load bearing capacity of the specimen, and the sudden changes in load would have been smaller, thus producing a smoother force-extension curve.

ASTM D5961 [90] recommends that each test be run until a clear maximum load is reached. However, it is clear from dips in force-extension curves (and from the cracking noises observed during the tests) that fibres had begun failing before a maximum load was observed. When considering the strength of the bolted joint, it would be of greater value to consider the elastic load. This was defined as the point where the change in the slope is greater than 20% of the original slope, which was assumed to be the onset of permanent damage, where individual fibres have begun failing. An alternative to this would be setting a strain failure criterion where the specimen is be considered to have failed at a certain value of strain. Strain failure criteria in composites typically have limits of 1-3% maximum allowable strain.

5 Hybrid joining [CL]

The bonding fastener selected for study consists of a threaded stud joined to a perforated metal plate by projection welding [17]. The base of the fastener is bonded onto the surface of one of the parts to be joined, while the stud of the fastener is secured with a nut through a hole in the second part. Figure 5 shows an assembly where a bonding fastener is used to join two laminates in a single lap configuration. The laminates are loaded by a tensile force (F).

In the absence of established theoretical models of this type of joint, an experimental approach to analysis was taken. The joint was split down into three constituent components:

1. The adhesive joint between the first laminate and the fastener base
2. The fastener, including the weld at stud root, and the stud itself
3. The drilled hole in the second laminate (as analysed in Section 4)

An experimental programme was designed and carried out to isolate the behaviour of each component, with the aim of understanding the overall mechanics of the joint. A final set of tests was then carried out on full hybrid joints.

5.1 Laminate-to-fastener bond [CL]

Mechanical tests of adhesive single lap joints were carried out according to ASTM D5868 [56] to investigate the adhesive bond between the laminate and the bonding fastener base. Bonded assembles were made with one carbon-epoxy laminate adherend and one perforated steel adherend. The assemblies were mounted in a universal testing machine and loaded statically in tension.

5.1.1 Specimens and method [CL]

Figure 43 shows schematics of the two adherends that were bonded to form adhesive joints. The adherend shown in Figure 52a is the same as the 2mm adherends described in Section 3.4. The adherend shown in Figure 52b was made by cutting 316 stainless steel sheet into strips, and then drilling holes in a pattern to replicate the bonding fastener base. The methacrylate adhesive investigated in Section 3.4 was used to bond the two adherends. An excess of adhesive was applied to ensure that all holes in the metal were filled.

Figure 44 shows the geometry of the specimens produced. To represent the dimensions of the fastener base, the overlap length and width were assigned a nominal value of 32mm, and 1.2mm-thick steel was used. However, in preliminary tests with 1.2mm-thick

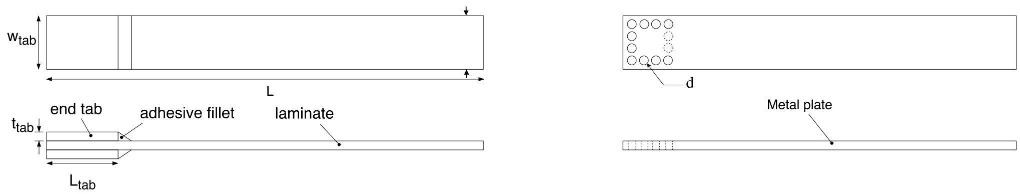

(a) Laminate (b) Steel

Figure 43: Adherends bonded to produce the laminate-steel adhesive joint specimens

steel adherends, all trial specimens failed by tensile failure (defined in Figure 30) in the steel. To mitigate this, 2mm-thick steel was used, and only two holes were drilled at the top edge (shown as dotted circles in Figure 52b) so as to reduce the likelihood of necking. This meant that the specimens represented geometry of the fastener base less well than before. However, it was a necessary change in order to increase the likelihood of failure in the adhesive layer rather than in the adherends.

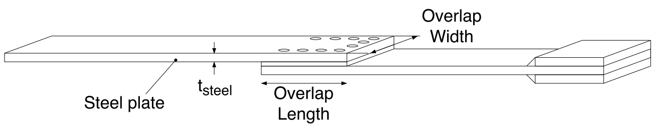

Figure 44: Specimen geometry used in mechanical tests of laminate-steel adhesive joints

Measurements were taken to quantify manufacturing variations. These are summarised in Table 27, which presents mean ($\bar{x}$) and standard deviation (s) values to the resolution of the calipers used (0.01mm).

w	L	t_{steel}
31.85 ± 0.10	32.56 ± 0.46	1.90 ± 0.04

Table 27: Measured dimensions ($\bar{x} \pm s$ in mm) of the laminate-steel adhesive joint specimens

The same test method as described in Section 3.4 was used for five specimens.

5.1.2 Results [CL]

The average adhesive shear stress (τ_0) was calculated by normalising the tensile force with respect to the bond area (see Equation 28), thus accounting for manufacturing variations. The longitudinal strain of the joint (ϵ) was calculated by finding the change in distance (Δ) between the extensometer arms, and normalising with respect to the distance before loading (L_0), as in Equation 18. Figure 45a shows plots of the tensile force in the specimen with increasing grip separation. Figure 45b shows plots of τ_0 plotted against ϵ.

Irregular changes in the measured values from the clip-on extensometer indicated that

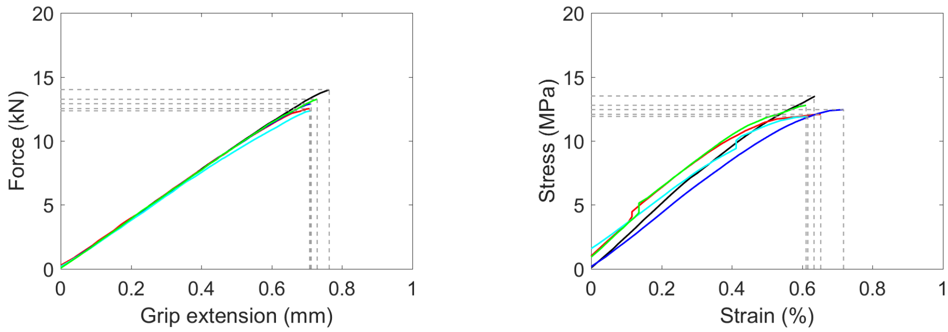

(a) Force-extension

(b) Stress-strain

Figure 45: Experimentally determined longitudinal tensile force-extension and stress-strain responses of laminate-steel adhesive joint specimens

the instrument slipped on the surface of the specimens. The results were post-processed to reduce the effects, but some artefacts of this error remain visible in Figure 45b.

Table 28 presents the sample mean ($\bar{x}$) and standard deviation (s) for failure stress (τ_f) and failure strain (ϵ_f) before and after post-processing. The results were tested for outliers using the Peirce criterion. No outlying data sets were found. Shown for comparison are the values calculated from the results for the 2mm laminate adhesive joints (Section 3.4). All five specimens failed in the composite adherend, ranging from light to mild fibre tear.

Adherends	τ_f **(MPa)**	ϵ_f **(%)**
Laminate & metal	12.54 ± 0.63	0.62 ± 0.04
Laminate	14.04 ± 0.43	0.34 ± 0.03

Table 28: Experimentally determined failure stress and strain ($\bar{x} \pm s$) of laminate-steel adhesive joint specimens

5.1.3 Discussion [CL]

It can be seen in Table 28 that, compared with joints with only laminate adherends, the joints with metal and composite adherends failed at lower adhesive shear stress and higher joint strain values. This is likely to be due to the combination of dissimilar materials. As the two adherends are not rigidly attached, the different Poisson's ratios and Young's moduli of the adherends may lead to increased stress in the adhesive layer.

The method used to post-process the test data was judged to be the most sensible way to correct for slipping of the extensometer. A better method would have been to find the extension at each step to compute the real difference. However, this information was unavailable due to how data were recorded by the testing machine. Instead of a constant rate of data recording, the system reduced the overall number of data points by only recording values that represented a certain percentage change from the previous value. To prevent extensometer slip in future experiments, it is suggested that both faces of the metal adherend could be abraded to increase surface roughness.

5.2 Bonding fastener [CL/AV]

In order to study the bonding fastener (see Figures 5 and 46) in isolation, it was considered as a cantilever loaded by a force on its threaded section (see Figure 47).

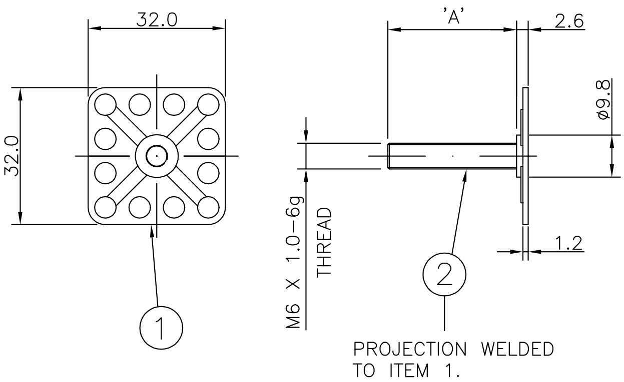

Figure 46: Geometry (dimensions in mm) of the bonding fastener (from [101])

Three potential failure modes were identified. First, it could fail in the weld between the base plate and the threaded stud. Second, it could fail at the base of the threaded stud due to a bending moment. Third, it could fail by shearing at the point where it is loaded by the drilled hole in the laminate. In order to predict how the fastener would fail in the full hybrid joint assembly, all three failure modes were investigated to estimate the load at which they would be expected to occur.

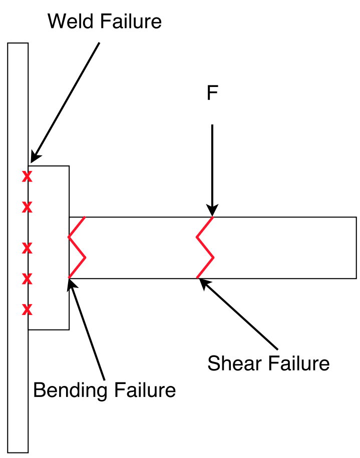

Figure 47: Potential failure modes of the bonding fastener loaded on its threaded stud

5.2.1 Theoretical analysis of weld at fastener base [FBS]

The bonding fasteners studied were manufactured by projection welding a threaded stud to a perforated metal base plate [17]. In this welding process, two electrodes apply a closing pressure on the components to be joined, and a potential difference is applied across them. An X-shaped embossment (or 'projection') on the metal plate localises the resultant electrical current through the components, causing small regions of the material to heat up by ohmic resistance. This heating is sufficient to soften and fuse the two mating components [93]. Figure 48 illustrates the welding process.

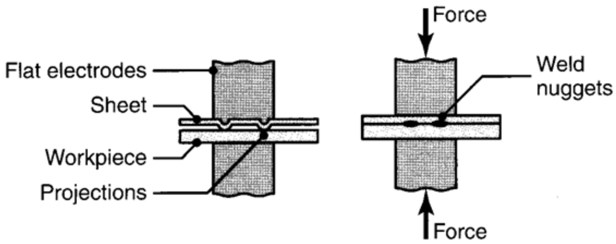

Figure 48: Schematic of the projection welding process (from [94])

Considering the fastener as a cantilever, the reaction at the weld consists of a shear force, $V = F$, and a bending moment, $M = FL$, where L is the distance from the weld to the point of force application. The shear force produces a primary shear stress, τ', while the moment produces a secondary shear stress, τ''. The resultant shear stress, τ, in the weld is the Pythagorean combination of τ' and τ''. The magnitudes of these stresses are given by

$$\tau' = \frac{V}{A} \qquad \tau'' = \frac{Mr}{I} \qquad \tau = \sqrt{\tau'^2 + \tau''^2} \tag{49}$$

where A is the area of the weld, r is the radius of the weld, and I is the second moment of area of the weld about its centroid [53].

The geometry of the weld area was approximated by finding the intersection of the X-shaped projection with the circular cross-section of the threaded stud (see Figure 49). The values of A and I, also shown in Figure 49, were calculated using Autodesk Inventor [95]. Using these values, the stresses in the weld can be calculated using Equation 49:

$$\tau' = \frac{V}{A} = \frac{F}{A} = \frac{F}{51.35} = 0.0195F$$

$$\tau'' = \frac{Mr}{I} = \frac{Flr}{I} = \frac{F \times 7.4 \times (9.8/2)}{254.97} = 0.1422F$$

$$\tau = \sqrt{0.0195^2F^2 + 0.1422^2F^2} = 0.1435F$$

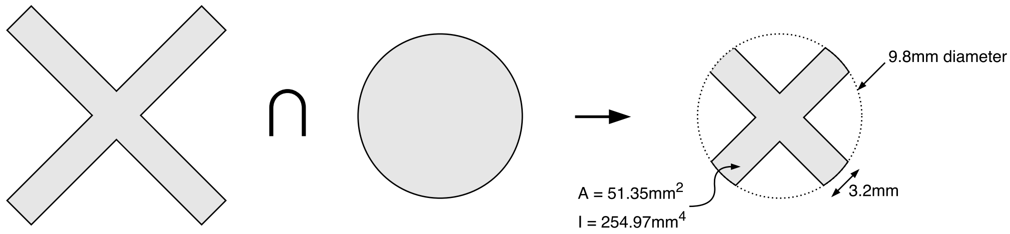

Figure 49: Geometry used to approximate the area of the weld

Using the ultimate tensile strength for 316 stainless steel (S_u = 550MPa [12]), the predicted maximum loading capacity of the weld was found to be

$$F_{max} = \frac{S_u}{0.1435} = \frac{550}{0.1435} = 3.8\text{kN} \tag{50}$$

Important simplifications were made in arriving at this estimate. First, it was assumed that the strength of the material is unchanged by the welding process. In reality, the heat used in welding does cause metallurgical changes. Annealed stainless steel contains carbon in solid solution with iron-chromium-nickel alloy. At temperatures between 426°C and 760°C, the carbon tends to join with the chromium at grain boundaries, forming chromic carbide in a process of 'carbide precipitation'. This reduces the strength of the steel [96].

The extent to which precipitation occurs depends on the length of time for which the metal is held in the critical temperature range. Projection welding is a fast process, and only a small volume of metal is heated, so the effect was accepted to be negligible. Carbide precipitation is also dependent on the carbon content of the alloy. This is low in 316 stainless steel (less than 0.03% [12]), so the metal has relatively low susceptibility to this form of degradation [96]. Therefore, the assumption of unchanged strength was judged to be acceptable.

A second assumption was that residual stresses can be neglected. These are stresses that exist in the material in the absence of external loading. Their effect is to reduce the amount of applied stress required to induce material failure [97]:

$$\text{total stress} = \text{residual stress} + \text{applied stress} \tag{51}$$

The welding process used may result in residual stresses. The material in the weld area is heated rapidly, and expands as a result. The colder surrounding material restrains this expansion, causing thermal stresses. These stresses partly exceed the yield limit, which is reduced at elevated temperatures, and the weld area is compressed plastically. As it cools, the material in the weld area contracts, resulting in tensile residual stress. The stress in the surrounding material is compressive [98]. These effects result in a distribution of residual stress similar to that shown in Figure 50, which presents the findings of Watanabe and Sato [99]. Although their work focussed on plug welds, the stress distribution around the approximately circular projection weld considered could be expected to be similar [98].

Due to the small size of the parts being welded, it was assumed that all regions heat up and cool quickly, thus giving shallow temperature gradients in the material. Therefore, thermal residual stresses were assumed to be insignificant.

In some cases, the clamping forces applied during the welding process may also induce residual stresses [53]. Because the perforated steel base is thin (1.2mm [100]), any significant clamping-induced stresses could be expected to cause geometric distortion of the finished part. Under visual inspection, no such distortion was found in the bonding fasteners. Therefore, it is concluded that the residual stresses in the finished parts were not significant.

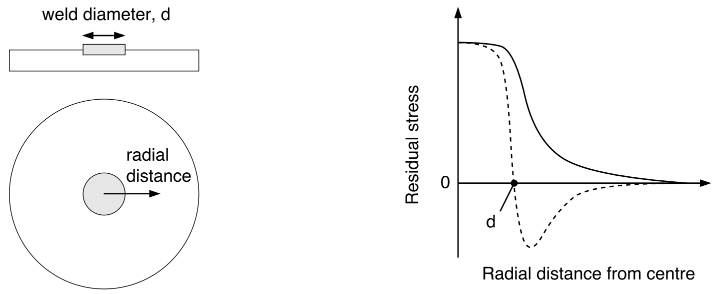

Figure 50: Schematic plot of the distribution of radial (solid) and tangential (dashed) residual stress around a plug weld in a circular plate [98]

5.2.2 Theoretical analysis of threaded stud [AV]

The failure of the stud component of the bonding fastener was investigated. The stud was considered as a smooth, cylindrical beam of diameter $d = 5.32$mm equal to the pitch diameter of an ISO M6 threaded stud [82]. The maximum bending stress in a cylindrical beam can be expressed as

$$\sigma_{bmax} = \frac{Mr}{I} \tag{52}$$

where M is the bending moment at the fixed end of the stud, r is the radius of the cross-section of the stud, and I is the second moment of area of the cross-section [53]. The bending moment can be expressed as $M = FL$, where F is the applied load, and L is the distance from the point of interest to the point of force application. A value of $L = 3.6$mm was found by analysing the geometry of the hybrid joint assembly.

Using the ultimate tensile strength (S_u) of the fastener material, the load at which failure is expected at the stud base is given by

$$F_{max} = \frac{S_u I}{rL} = \frac{515 \times \pi \times 2.66^4}{4 \times 2.66 \times 3.6} = 2.1\text{kN} \tag{53}$$

Alternatively, the threaded stud could fail by shearing at the interface with the drilled hole in the laminate. Assuming a negligible bending moment, the average shear stress (τ) in the stud can be stated as

$$\tau = \frac{F}{A} \tag{54}$$

where F is the load on the stud, and A is the cross sectional area of the stud. The thread of the stud reduces its effective cross-sectional area (see Figure 51). Thus A was calculated based on the minor diameter of an ISO M6 threaded stud (d = 4.89mm) [82].

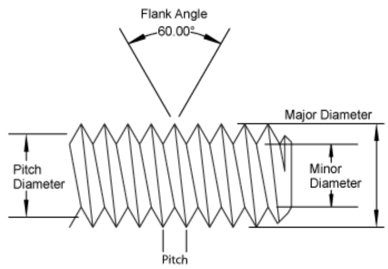

Figure 51: Schematic of a screw thread on a mechanical fastening element (from [81])

The maximum shear stress in a circular beam is given by [80]

$$\tau_{max} = \frac{4}{3}\tau \tag{55}$$

Combining Equations 54-55, and setting $\tau_{max} = S_u$, the failure load can be expressed as

$$F_{max} = \frac{3}{4}AS_u = \frac{3}{4} \times \pi \times 2.445^2 \times 515 = 7.3\text{kN} \tag{56}$$

5.2.3 Experimental analysis [CL]

An experiment was designed with reference to ASTM F606 [91] to test the strength of bonding fasteners in shear.

Specimens and method [CL/AV]

Figure 52 shows a schematic of the specimens used to test the bonding fasteners. Each bonding fastener was bolted through the holes in its base to a 6mm-thick steel plate. A shear load was applied to the threaded stud by another 6mm-thick steel plate, which had a hole drilled on its centreline for assembly with the bonding fastener. The nut was tightened to the point where it just made contact with the metal plate, with no additional torque applied to it. This was to avoid contact (and, thus, friction) between the right-hand metal plate and the heads of the bolts.

Five specimens were tested. In each test, free ends of the metal plates were mounted in the grips of a universal testing machine. An engineer's square was used to ensure that the plates and the specimen were straight and in line with the loading axis of the machine. The grips were separated at a cross-head speed of 6mm/min. The tensile force in the specimen was measured using a 100kN load cell.

(a) Exploded view

(b) Side view

Figure 52: Assembly used in mechanical tests of bonding fasteners

Results [AV]

Figure 53 shows the variation in measured tensile load with increasing grip separation. The maximum load in each data set was found. In addition, the elastic limit was identified. In order to achieve this, the gradient in a linear range (grip extension of 0.2-0.9 mm by visual inspection) was calculated. The elastic limit was then defined as the point at which the gradient of the force-extension curve changes by more than 20% of the linear gradient.

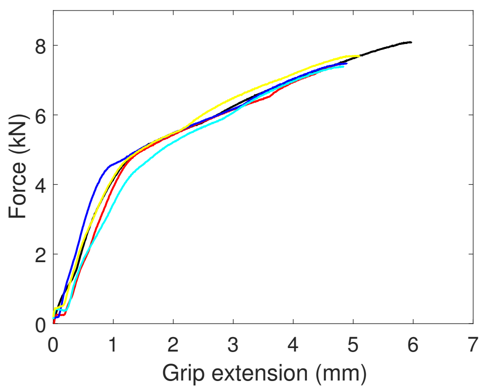

Figure 53: Experimentally determined longitudinal tensile force-extension responses of bonding fastener specimens

Applying the Peirce criterion as described in Section 2.2 revealed that one specimen produced results that did not conform with the rest. After eliminating the outlier, the sample mean ($\bar{x}$) and standard deviation (s) were re-calculated for load and extension at the elastic limit (F_e and X_e respectively), and for maximum load (F_{max}) and corresponding extension (X_{Fmax}). These are presented in Table 29.

F_e (kN)	X_e (mm)	F_{max} (kN)	X_{Fmax} (mm)
4.52 ± 0.03	1.17 ± 0.16	7.53 ± 0.11	4.92 ± 0.11

Table 29: Experimentally determined tensile load and machine grip extension ($\bar{x} \pm s$) at the elastic limit and at the point of maximum load of bonding fastener specimens

5.2.4 Discussion [AV]

Based on theoretical analysis, it was predicted that failure would occur in the weld between the fastener base and the threaded stud. In fact, four out of the five bonding fasteners tested failed by shearing at the root of the threaded stud, while one failed due to shearing of the base plate.

The most likely explanation for the difference between the predicted and actual failure loads is the assumption that the three failure modes are independent. In reality, the base of the stud and the weld are not loaded purely in shear or in bending but in a combination of both. In addition, the base of the fastener deformed under loading despite being fastened to the metal plate with eight bolts. This changed the geometry of the fastener and, therefore, the load path through it.

The maximum load predicted theoretically for shear failure of the stud was within 5% of the mean experimental value. It can be concluded that assuming this failure mode results in the best prediction of the failure load of an isolated bonding fastener under shear loading on its stud.

5.3 Full hybrid joint [CL]

An experiment was designed with reference to ASTM D5868 [56] and ASTM D5961 [90] to test the strength of hybrid joints between laminates loaded in tension.

5.3.1 Specimens and method [CL]

The specimens were made by assembling two parts. A schematic of the first part (A) is shown in Figure 54. The second part (B) was of the same geometry as shown in Figure 38. The assembly was secured using a nut (see Figure 5).

The nominal dimensions of part B can be found in Table 22. The same nominal laminate width, length and thickness were used for part A. Measurements of the actual dimensions are summarised in Table 30, in which w_{stud} denotes the width of part A at the joint, w_{hole} denotes the width of part B at the joint, L denotes the length of the parts, d denotes the diameter of the hole in part B, e denotes the distance of the hole centre in part B from the top edge, and s denotes the distance of the hole centre in part B from the right edge. Mean ($\bar{x}$) and standard deviation (s) values are stated.

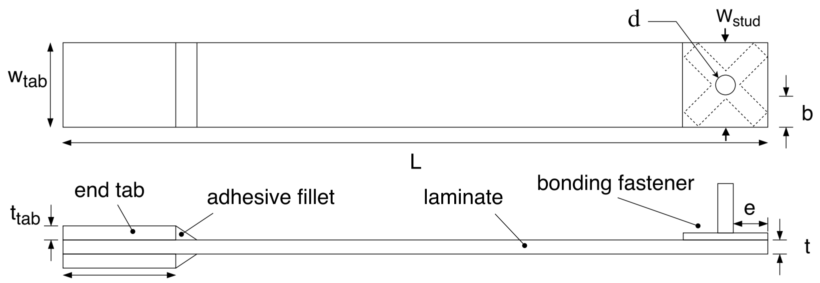

Figure 54: Part A of the specimens used in mechanical tests of full hybrid joints

The nominal dimensions of part B can be found in Table 22. The same nominal laminate width, length and thickness were used for part A. Measurements of the actual dimensions are summarised in Table 30, in which w_{stud} denotes the width of part A at the joint, w_{hole} denotes the width of part B at the joint, L denotes the length of the parts, d denotes the diameter of the hole in part B, e denotes the distance of the hole centre in part B from the top edge, and s denotes the distance of the hole centre in part B from the right edge. Mean ($\bar{x}$) and standard deviation (s) values are stated.

w_{stud}	w_{hole}	L	d	e	s
32.20±0.14	32.05±0.09	145.68±0.38	6.01±0.01	15.87±0.29	15.56±0.24

Table 30: Measured dimensions ($\bar{x} \pm s$ in mm) of full hybrid joint specimens

Five specimens were assembled and tested in a universal testing machine. The machine grips were separately longitudinally at a cross-head speed of 2mm/min. This speed was the lower of the two values found when consulting the ASTM standards used, and was selected to minimise strain rate-related effects in the response of the specimens. Due to the thickness of assembled specimens, the clip-on extensometer could not be used.

5.3.2 Results [CL]

Figure 55 shows the variation in measured tensile load with increasing grip separation. One outlier was identified using the Peirce criterion. Table 31 presents the sample mean ($\bar{x}$) and standard deviation (s) values of failure load and extension re-calculated after eliminating this outlier.

Failure load (kN)	Extension at failure (mm)
2.34 ± 0.13	1.62 ± 0.12

Table 31: Experimentally determined tensile load and machine grip extension ($\bar{x} \pm s$) at the elastic limit and at the point of maximum load of full hybrid joint specimens

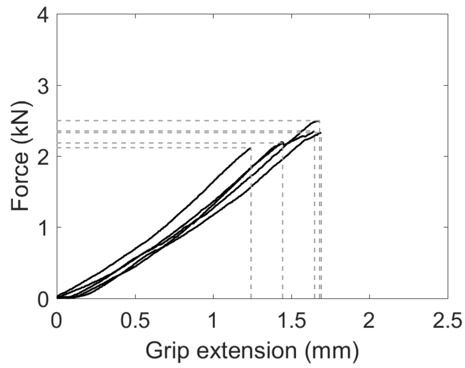

Figure 55: Experimentally determined longitudinal tensile force-extension responses of full hybrid joint specimens

5.3.3 Discussion [CL]

If a 'weakest link' approach were used to predict the behaviour of a full hybrid assembly, it would be expected, with reference to Table 32, that failure would occur first in the pin-loaded hole in the assembly, and at a tensile load of approximately 5.41kN. In fact, all of the full hybrid joints failed in the adhesive layer, and at a mean maximum load of 2.34kN.

Assembly component	**Failure load (kN)**
Laminate in tension	27.20
Adhesive in shear	11.16
Fastener stud in shear	7.53
Pin-loaded hole in laminate	5.41

Table 32: Comparison of experimentally determined failure load of each component of the hybrid joint

The over-estimation of joint strength was a result of assuming that each component acts the same in the assembly as in isolation. In particular, the effects of loading eccentricity were significantly under-estimated when analysing the adhesive bond between the laminate and the fastener base. Due to the geometry of the bonding fastener, the drilled laminate could not be located close to the base. Thus, there was a significant perpendicular distance between the loading axis and the adhesive layer, causing a large peel load.

6 Discussion [FBS/CL/AV]

The key findings of theoretical and experimental analyses are presented. An approach to selecting a joining method is suggested. Guidelines for the design and analysis of joints are proposed.

6.1 Summary of findings [FBS/CL/AV]

For adhesive joints, Allman's solution was found to be the closed-form model that best predicted the experimentally determined strength. In the case of joints between 2mm-thick laminates, a theoretical-experimental deviation of 23% was found. The accuracy of the theoretical analysis was limited by the representation of adherend material properties, the idealisation of joint geometry, and the availability of the information about adhesive material properties.

For mechanically fastened joints, assuming material isotropy produced the most accurate theoretical predictions, with an 8% deviation from experimental results. Using the Yamada failure criterion resulted in more significant underestimation of actual joint strength. It is suggested that this method would be more accurate for unidirectional laminates, however. For hybrid joints, the analytical approach taken resulted in an overestimation of actual strength by 131%. Investigating the components of the joint in isolation before applying a weakest link failure criterion was limited in accuracy because the interactions between the components were neglected.

Figure 56 shows a comparison of typical responses of each joint type to static tensile loading. Adhesive joints were found to have the greatest strength. They failed suddenly and at low values of longitudinal extension. Mechanical joints had lower strength, but failure was considerably more gradual. Hybrid joints failed suddenly and at relatively low loads. The effective stiffness of the joints can be inferred from the gradient of the force-extension curves in Figure 56. Adhesive bonding produced the stiffest joints, while hybrid joining produced the least stiff.

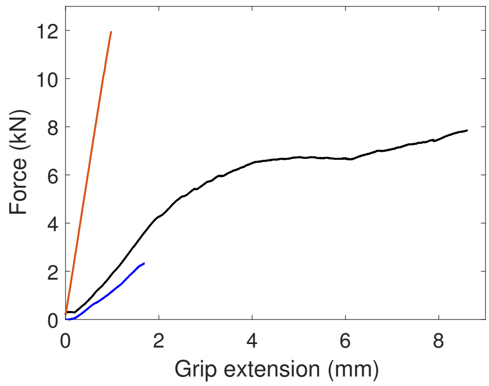

Figure 56: Typical responses of adhesive joints (red), mechanically fastened joints (black) and hybrid joints (blue) to tensile loading of the laminates being joined

Adhesive joints were found to be more sensitive to manufacturing inconsistencies than both mechanically fastened and hybrid joints. The standard deviation of the experimental failure load results was 9% of the mean for the adhesive joints (with 2mm-thick adherends), 2% of the mean for mechanically fastened joints, and 6% of the mean for hybrid joints.

6.2 Approaches to analysis [FBS]

Three approaches were taken to analysing the strength of joints. Closed-form algebraic solutions were found to offer fast and generally intuitive predictions, making them valuable for preliminary design calculations. More general solutions tended to provide greater accuracy to empirical results at the expense of ease of use. Therefore, for design purposes, a trade-off should be sought to maximise the utility of the model.

Finite element analysis was a valuable alternative for making theoretical estimates. It allowed materials to be defined more completely than in closed-form models, which was shown to be significant for the anisotropic materials investigated. Furthermore, it included physical effects that were neglected in other models to produce simple algebraic expressions. As is generally true for all theoretical analyses, both closed-form and finite element analyses were fundamentally limited by the accuracy of the values used as inputs. The information provided by manufacturers was found to be inadequate in a number of instances throughout the project.

For the simple joints considered, experimental analysis is likely to have been the best representation of the joints that would be used in practice. Of particular importance was the fact that it highlighted the physically significant effects of manufacturing variations. However, the utility of experimental analysis is limited by the extent to which the expected loading state can be replicated in a laboratory environment. In turn, this is limited by the available testing equipment. As a result, mechanical testing setups typically over-idealise the loads on a joint, and it is difficult to test more complex joint configurations. Finally, experimental analysis of joint strength requires that specimens be manufactured and tested to destruction. Thus, it was time- and resource-intensive.

Analysing joints both theoretically and experimentally provided greater insight than would have been achieved with either approach alone. Experimental results validated the predictions of theory, while theory served to explain physical phenomena. With sufficient confidence in theoretical models, the amount of experimental validation required might be reduced in future work.

6.3 Joining method selection [FBS]

Even with sufficient information on which to base decisions, it may not be clear which joining method is the most suitable for a given design scenario. In order to support decision-making, a comparison can be made with respect to a set of criteria that represent the key concerns of the designer.

To identify a set of design criteria for joining methods, the typical life cycle of a joint – from design and analysis at the early stages to recycling, reuse or disposal at the end of life – was analysed (see Tables 34-36 in Appendix B). Using this systematic approach increased the likelihood of producing an exhaustive set of design criteria. Similarity with other criteria sets in the literature [19, 13, 57] validated this process.

The Pugh concept selection method [102] was used to demonstrate how the suggested criteria can be used to determine which joining method best satisfies the requirements of a given design scenario. In this decision-making approach, one of the candidate designs is used as a datum. The alternatives are then compared to the datum with respect to each of the design criteria.

The knowledge acquired over the course of the project was used to make judgements on the relative performance of adhesive bonding, mechanical fastening and hybrid joining. While there was good knowledge of some aspects of the joining methods (such as performance under shear loading), there was high uncertainty associated with some other judgments (such as performance under impact loading). Therefore, a coarse scoring scale was used. Using adhesive bonding as the datum, mechanical fastening and hybrid joining were either judged to be better (score of +1), the same (score of 0) or worse (score of -1) with respect to each design criterion (see Tables 34-36). Future selection processes are likely to be based on a stronger knowledge base, in which case it might be decided to use a finer scale (such as -10 to +10).

Attempting to generalise the design requirements of a Formula Student team proved problematic due to the different priorities of subgroups within the team. For example, a subgroup focussed on long-term design changes might be more concerned with the mechanical performance of a joint than the lead time when procuring components. A subgroup in charge of preparing the car for race track events might be most concerned with the ease of inspection, disassembly and repair. Therefore, a demonstration case with a specific decision-maker and design scenario was considered.

Tables 34-36 present judgments as to the design priorities of a track-side maintenance team tasked with joining a front wing assembly to the nosebox (see Figure 1). Each criterion was assigned a binary value denoting importance to the decision-maker. The overall merit of both mechanical fastening and hybrid joining relative to adhesive bonding was found by summing the product of each score with the corresponding importance value. Mechanical fastening was found to be the joining method of preference, following by adhesive bonding and hybrid joining.

The Pugh method was selected for this demonstration because it presents the comparison of candidates in a way that is simple to interpret. However, it has been criticised. Hazelrigg [103] put forward a compelling case against the use of this method, showing that it can recommend considerably suboptimal designs. Therefore, the results of this analysis are likely to have limited value. Despite this, the design criteria identified may be useful in conjunction with an alternative decision-making method. A review of such techniques is suggested.

6.4 Evaluation of key decisions [FBS/CL/AV]

The decision to study carbon-epoxy laminates was based on the current use of this material in the Formula Student car, and the aim to provide useful information to designers. This choice of material also made it possible to procure professionally manufactured sheets of laminate, ensuring greater consistency than would have likely been achieved by production at the university. Based on previous work investigating the use of carbon fibre-reinforced epoxy in Formula Student [8], 2mm-thick laminates with a 5-ply quasi-isotropic lay-up were used for the comparison of joining methods. These material selection decisions were, therefore, based on sound reasoning. However, the use of laminates with woven fabric plies made theoretical analysis more difficult than if unidirectional plies had been used.

Single lap joints were identified as the configuration most extensively covered in the literature, thus enabling detailed theoretical analysis. They were also selected for their ease of manufacture and testing, which proved to be acceptably straightforward. An argument could be made in favour of studying double lap joints instead, based on the possibility that theoretical analysis would have been simpler (with reduced bending effects). This would have been more time- and resource-intensive, however, requiring the manufacture of more laminate components.

Both adhesive bonding and mechanical fastening were selected for investigation because neither one was obviously preferable to the other in all respects (see Table 1). No evidence was found to suggest that mechanical fasteners other than bolts should be used. A consideration of the mechanics of single lap joints might have resulted in the selection of an alternative hybrid joint configuration to the one that was studied. However, this decision was based on limited knowledge in the early stages of the project. The investigation into hybrid joining provided insight nevertheless. It clearly demonstrated the importance of using a joint configuration that minimises peel loads in the adhesive layer.

The joints were considered for the case of static tensile loading in the laminates. As was true for other decisions, part of the rationale for this was the existence of previous work on which to base this project. Also considered was the ability to test the joints with the equipment available. Tensile loading was simple to achieve with a universal testing machine. Other loading cases could have been validly selected for investigation.

6.5 Future work [FBS/CL/AV]

Further investigation into the material properties of laminates, with particular attention paid to through-thickness properties and woven architectures, would likely lead to better predictions of joint strength. The principles of analysis used in this project could be expected to apply to joints between other continuous fibre-reinforced plastic laminates. If composites with thermoplastic matrices were of interest, additional joining techniques such as fusion bonding [104] may be considered. Alternatively, an investigation could be made into methods of joining sandwich structures. The Formula Student team intends to use these in the future manufacture of a monocoque chassis [8].

Other joint configurations, such as double lap joints or stepped lap joints, could be investigated. However, given the likelihood of using single lap joints in the Formula Student car, better characterisation of this configuration under different loading modes might be more useful.

Perhaps the most valuable development of the theoretical analysis of adhesive joints would be refining the finite element model used. The key considerations should be material stress-strain nonlinearity and failure, and the effects of adhesive fillets. Residual thermal strains from adhesive curing may also be of interest. The strength of bolts in shear was not found to be a limiting factor in the strength of mechanically fastened joints. Therefore, there is no requirement to investigate alternative mechanical fasteners for the purpose of increasing joint strength. However, alternatives may be considered if they offer improvements with respect to other design criteria. For example, certain rivets might provide a suitable but more lightweight method of mechanical fastening. Variations on the mechanically fastened and hybrid joints considered may better suit certain design scenarios. For example, multi-fastener arrays and different ways of incorporating bonding fasteners (such as embedding in the composite lay-up before curing) could be investigated.

7 Conclusions [FBS/CL/AV]

The aim of the project was to investigate methods of joining fibre-reinforced plastics in the context of Formula Student. Three methods of joining carbon-epoxy laminates – adhesive bonding, mechanical fastening, and hybrid joining – were analysed theoretically and experimentally. In mechanical tests of single lap joints, adhesive bonding was found to provide the greatest strength and stiffness, followed by mechanical fastening and, last, hybrid joining. The onset of failure was considerably more gradual in mechanically fastened joints than in the other joint types. Mechanical fastening produced the most consistent joints in terms of failure load.

The approaches taken to analysis provided varying degrees of insight into the mechanics of joints. Algebraic solutions allowed for quick and intuitive calculations, but were limited by the simplifications on which they were based. Finite element analysis allowed for better representation of anisotropic materials, and demonstrated the deformation of joints under loading. Experimental analysis accounted for the effects of manufacturing variability that would be expected in Formula Student.

Suggestions were made for how to select a joining method for a specific design scenario. Based on limited knowledge, a decision-making technique was demonstrated. This process revealed the limitations associated with incomplete information and unclear design objectives.

Future work should be carried out with the aim of more extensively characterising the joining methods and materials studied. Considering different loading scenarios and variations on joint configurations would increase the amount of useful information available to designers. This, combined with more developed theoretical models, would enable future Formula Student teams to more effectively approach the problem of joining fibre-reinforced plastics.

References

[1] Mallick, P (2007) *Fiber-Reinforced Composites: Materials, Manufacturing, and Design*, Third Edition. Taylor & Francis.

[2] Campbell, F (2006) *Manufacturing Technology for Aerospace Structural Materials*. Elsevier.

[3] O'Rourke, B (1990) The uses of composite materials in the design and manufacture of Formula 1 racing cars. *Proceedings of the Institution of Mechanical Engineers*, 204. IMechE.

[4] Savage, G (2010) Formula 1 composites engineering. *Engineering Failure Analysis*, 17. Elsevier.

[5] Hull, D & Clyne, T (1996) *An Introduction to Composite Materials*, Second Edition. Cambridge University Press.

[6] Kelly, G (2004) *Joining of Carbon Fibre Reinforced Plastics for Automotive Applications*. PhD thesis. KTH Royal Institute of Technology.

[7] Hexcel Composites (1997) *Prepreg Technology*.

[8] McCalla, A, Cameron, C, Foster, G & Hollington, R (2016) *Study into the Design and Manufacture of a CFRP Monocoque Chassis for Formula Student*. University of Bristol.

[9] Institution of Mechanical Engineers (2017) *Formula Student*. Available from formulastudent.imeche.org/formula-student [accessed April 2017].

[10] Matthews, F (1987) *Joining Fibre-Reinforced Plastics*. Elsevier Applied Science.

[11] Swift, K & Booker, J (2003) *Process Selection: from Design to Manufacture*, Second Edition. Butterworth-Heinemann.

[12] Granta Design (2016) *CES EduPack 2016*.

[13] Åström, B (1997) *Manufacturing of Polymer Composites*. CRC Press.

[14] Adams, R, Comyn, J & Wake, W (1997) *Structural Adhesive Joints in Engineering*. Chapman & Hall.

[15] Wichita State University (2012) *Composite Materials Handbook, Volume 3: Polymer Matrix Composites*. SAE International.

[16] European Space Agency (2011) *Space Engineering: Structural Materials Handbook, Part 2*. ESA Requirements and Standards Division.

[17] bigHead Bonding Fasteners (2017) *bigHead Bonding Fasteners*. Available from bighead.co.uk [accessed April 2017].

[18] Penn Engineering (2017) *PEM VariMount Bonding Fasteners*. Available from pemnet.com [accessed April 2017].

[19] Broughton, W, Crocker, L & Gower, M (2002) *Design Requirements for Bonded and Bolted Composite Structures*. HMSO.

[20] European Space Agency (2011) *Space Engineering: Adhesive Bonding Handbook*. ESA Requirements & Standards Division.

[21] Penalver, W (2017) RE: Rigid Carbon Fibre Sheet (One-Sided) [email].

[22] Easy Composites (2017) *Understanding Carbon Fibre Cloth Reinforcement*. Available from easycomposites.co.uk/#!/composites-tutorials/carbon-fibre- cloth-explained [accessed April 2017].

[23] Jones, R (1999) *Mechanics of Composite Materials*, Second Edition. Taylor & Francis.

[24] Mitsubishi Rayon (2013) *Pyrofil: Typical Properties of Carbon Fiber*.

[25] Toray Carbon Fibers America (2008) *T700S Data Sheet*.

[26] Mitsubishi Rayon (2010) *Grafil 34-700*.

[27] Easy Composites (2017) *IN2 Epoxy Infusion Resin*.

[28] Lindell, M (2011) *The Laminator*.

[29] Zhou, G, Green, E & Morrison, C (1995) In-plane and interlaminar shear properties of carbon/epoxy laminates. *Composites Science and Technology*, 55. Elsevier.

[30] Chan, A, Chiu, W & Liu, X (2007) Determining the elastic interlaminar shear modulus of composite laminates. *Composite Structures*, 80. Elsevier.

[31] ASTM International (2014) *ASTM D3039: Standard Test Method for Tensile Properties of Polymer Matrix Composite Materials*. ASTM.

[32] Adams, D & Adams, D (2002) *Tabbing Guide for Composite Test Specimens*. FAA.

[33] Peirce, B (1852) Criterion for the rejection of doubtful observations. *The Astronomical Journal*, 2. American Astronomical Society.

[34] Ross, S (2003) Peirce's criterion for the elimination of suspect experimental data. *Journal of Engineering Technology*, 20. American Society for Engineering Education.

[35] Crookston, J, Long, A & Jones, I (2005) A summary review of mechanical properties prediction methods for textile reinforced polymer composites. *The Journal of Materials: Design and Applications*, 219. IMechE.

[36] ASTM International (2016) *ASTM D4762: Standard Guide for Testing Polymer Matrix Composite Materials*. ASTM.

[37] Broughton, B & Gower, M (2001) *Preparation and Testing of Adhesive Joints*. HMSO.

[38] Kinloch, A (1987) *Adhesion and Adhesives: Science and Technology*. Chapman & Hall.

[39] Adams, R (1987) Theoretical stress analysis of adhesively bonded joints. In: Matthews, F (ed) *Joining Fibre-Reinforced Plastics*. Elsevier Applied Science.

[40] da Silva, L, das Neves, P, Adams, R & Spelt, J (2009) Analytical models of adhesively bonded joints, part 1: literature survey. *International Journal of Adhesion & Adhesives*, 29. Elsevier.

[41] Mathworks (2016) *MATLAB 2016a*.

[42] Volkersen, O (1938) Die nietkraftverteilung in zugbeanspruchten nietverbindungen mit konstanten laschenquerschnitten. *Luftfahrtforschung*, 15. Oldenbourg.

[43] Goland, M & Reissner, E (1944) Stresses in cemented joints. *Journal of Applied Mechanics*, 66. ASME.

[44] da Silva, L, das Neves, P, Adams, R, Wang, A & Spelt, J (2009) Analytical models of adhesively bonded joints, part 2: comparative study. *International Journal of Adhesion & Adhesives*, 29. Elsevier.

[45] Hart-Smith, L (1973) *Adhesive-Bonded Single-Lap Joints*. NASA.

[46] Zhao, X, Adams, R & Pavier, M (1990) A new approach to determining the bending moment factors in single lap joints. *Proceedings of Adhesion '90*. Plastics & Rubber Institute.

[47] Benson, N (1969) Influence of stress distribution on the strength of bonded joints. *Adhesion: Fundamentals and Practice*. Gordon & Breach.

[48] Matthews, F, Kilty, P & Godwin, E (1982) A review of the strength of joints in fibre-reinforced plastics, part 2: adhesively bonded joints. *Composites*, 13. Butterworth & Co.

[49] Allman, D (1977) A theory for elastic stresses in adhesive bonded lap joints. *Quarterly Journal of Mechanics and Applied Mathematics*, 30. Oxford University Press.

[50] Adams, R & Peppiatt, N (1973) Effect of Poisson's ratio strains in adherends on stresses of an idealized lap joint. *Journal of Strain Analysis for Engineering Design*, 8. Sage.

[51] Hart-Smith, L (1974) *Analysis and Design of Advanced Composite Bonded Joints*. NASA.

[52] Dassault Systèmes (2015) *Abaqus/CAE 2016*.

[53] Nisbett, J & Budynas, R (2006) *Shigley's Mechanical Engineering Design*, Eighth Edition. McGraw-Hill.

[54] Cook, R (1995) *Finite Element Modeling for Stress Analysis*. John Wiley & Sons.

[55] Adams, R & Mallick, V (1992) A method for the stress analysis of lap joints. *Journal of Adhesion*, 38. Taylor & Francis.

[56] ASTM International (2014) *ASTM D5868: Standard Test Method for Lap Shear Adhesion for Fiber Reinforced Plastic (FRP) Bonding*. ASTM.

[57] European Space Agency (2011) *Space Engineering: Adhesive Bonding Handbook*. ESA Requirements and Standards Division.

[58] Banea, M & da Silva, L (2009) Adhesively bonded joints in composite materials: an overview. *Journal of Materials: Design and Applications*, 223. IMechE.

[59] Baldan, A (2004) Adhesively-bonded joints and repairs in metallic alloys, polymers and composite materials: adhesives, adhesion theories and surface pretreatment. *Journal of Materials Science*, 39. Kluwer Academic Publishers.

[60] Campbell, F (2001) Secondary adhesive bonding of polymer-matrix composites. In: Miracle, D & Donaldson, S (eds) *ASM Handbook, Volume 21: Composites*. ASM International.

[61] The Met Office (2017) *UK Climate – Extremes*. Available from metoffice.gov.uk/public/weather/climate-extremes/#?tab=climateExtremes [accessed April 2017].

[62] Permabond (2014) *Permabond ET500 Two-Part Epoxy: Technical Data Sheet*.

[63] Easy Composites (2017) *VM100 Black 10min Methacrylate Adhesive: Technical Data Sheet*.

[64] Permabond (2014) *Permabond PT326 Polyurethane Adhesive: Technical Data Sheet*.

[65] MatWeb (2017) *MatWeb: Online Materials Information Resource*. Available from matweb.com [accessed April 2017].

[66] Lang, T & Mallick, P (1998) Effect of spew geometry on stresses in single lap adhesive joints. *International Journal of Adhesion & Adhesives*, 18. Elsevier.

[67] da Silva, L, Critchlow, G & Figueiredo, M (2008) Parametric study of adhesively bonded single lap joints by the Taguchi method. *Journal of Adhesion Science and Technology*, 22. Taylor & Francis.

[68] Dassault Systèmes (2015) *Abaqus 2016 Online Documentation*. Available from 50.16.225.63/v2016 [accessed April 2017].

[69] Adams, R (1989) Strength predictions for lap joints, especially with composite adherends: a review. *The Journal of Adhesion*, 30. Gordon & Breach.

[70] Schon, J (2004) Coefficient of friction and wear of a carbon fiber epoxy matrix composite. *Wear*, 257. Elsevier.

[71] Yamada, S (1978) Analysis of laminate strength and its distribution. *Journal of Composite Materials*, 12. Sage.

[72] Chang, F, Scott, R & Springer, G (1982) Strength of mechanically fastened composite joints. *Journal of Composite Materials*, 16. Sage.

[73] Collings, T (1982) On the bearing strength of CFRP laminates. *Composites*, 13. Elsevier.

[74] Zhang, K & Ueng, C (1985) Stresses around a pin-loaded hole in orthotropic plates with arbitrary loading direction. *Composite Structures*, 3. Elsevier.

[75] Collings, T & Beauchamp, M (1984) Bearing deflection behaviour of a loaded hole in CFRP. *Composites*, 15. Elsevier.

[76] Brown, K, Morrow, C, Durbin, S & Baca, A (2008) *Guideline for Bolted Joint Design and Analysis: Version 1.0*. Sandia National Laboratories.

[77] de Jong, T (1977) Stresses around pin-loaded holes in elastically orthotropic or isotropic plates. *Journal of Composite Materials*, 11. Sage.

[78] Kretsis, G & Matthews, F (1985) The strength of bolted joints in glass fibre/epoxy laminates. *Composites*, 16. Elsevier.

[79] Kerns, J (2016) *What's the Difference Between Bearing, Shear, and Tear-Out Stress?* Available from machinedesign.com/fasteners/what-s-difference-between-bearing-shear-and-tear-out-stress [accessed April 2017].

[80] Beardmore, R (2013) *Shear Stresses/Deflections in Beams in Bending*. Available from roymech.co.uk/Useful_Tables/Beams/Shear_stress.html [accessed April 2017].

[81] Peninsula Components (2017) *Screw Design Guide*. Available from pencomsf.com/screws-categories/screw-design-guide [accessed April 2017].

[82] Maryland Metrics (2012) *Metric Thread – Extended Thread Size Range (ISO)*. Available from mdmetric.com/tech/M-thead%20600.htm [accessed April 2017].

[83] Vasiliev, V & Morozov, E (2001) *Mechanics and Analysis of Composite Materials*. Elsevier Science.

[84] Farrow, I (2017) *Composites Design & Manufacture*. University of Bristol.

[85] Clyne, B (2008) *Mechanics of Fibre-Reinforced Composites*. Available from doitpoms.ac.uk/tlplib/fibre_composites/index.php [accessed April 2017].

[86] Zhou, S & Sun, C (1990) Failure analysis of composite laminates with free edge. *Journal of Composites, Technology and Research*, 12. Sage.

[87] Sun, C, Quinn, B, Tao, J & Oplinger, D (1996) *Comparative Evaluation of Failure Analysis Methods for Composite Laminates*. FAA.

[88] Paiva, J, Mayer, S, & Rezende, M (2006) Comparison of tensile strength of different carbon fabric reinforced epoxy composites. *Materials Research*, 9. SciELO Brasil.

[89] Hinton, M, Kaddour, A, & Soden, P (200) Predicting failure in fibre composites: lessons learned from the World-Wide Failure Exercise. *Society of Manufacturing Engineers Technical Papers*. HMSO.

[90] ASTM International (2013) *ASTM D5961: Standard Test Method for Bearing Response of Polymer Matrix Composite Materials*. ASTM.

[91] ASTM International (2016) *ASTM F606: Standard Test Method for Determining the Mechanical Properties of Externally and Internally Threaded Fasteners, Washers, Direct Tension Indicators, and Rivets*. ASTM.

[92] Patrick, R (1976) *Structural Adhesives with Emphasis on Aerospace Applications: Treatise on Adhesion and Adhesives, Volume 4*. Marcel Dekker.

[93] Gould, J (1993) Projection welding. In: Olson, D, Siewert, T, Liu, S & Edwards, G (eds) *ASM Handbook, Volume 6: Welding, Brazing, and Soldering*. ASM International.

[94] Rajasekaran (2015) *Mechanical Engineer's World: Projection Welding*. Available from mechscience.com [accessed April 2017].

[95] Autodesk (2016) *Autodesk Inventor 2017*.

[96] Resistance Welding Manufacturers' Association (2003) *Resistance Welding Manual*, Fourth Edition. RWMA.

[97] Masubuchi, K (1980) *Analysis of Welded Structures: Residual Stresses, Distortion, and their Consequences*. Pergamon Press.

[98] Radaj, D (1992) *Heat Effects of Welding: Temperature Field, Residual Stress, Distortion*. Springer-Verlag.

[99] Watanabe, M & Sato, K (1954) Thermal stress and residual stress of circular plate heated at its centre. *Journal of Zosen Kiokai*, 86. The Society of Naval Architects of Japan.

[100] bigHead Bonding Fasteners (2004) *316 Blind Perforated Plate*.

[101] bigHead Bonding Fasteners (2008) *316-B32 Stud Fastener*.

[102] Lewis, K, Chen, W & Schmidt, L (2006) *Decision Making in Engineering Design*. ASME Press.

[103] Hazelrigg, G (2010) The Pugh controlled convergence method: model-based evaluation and implications for design theory. *Research in Engineering Design*, 21. Springer.

[104] Yousefpour, A, Hojjati, M & Immarigeon, J-P (2004) Fusion bonding/welding of thermoplastic composites.*Journal of Thermoplastic Composite Materials*, 17. Sage.

A Adhesive selection table

Table 33 was used to select adhesives for experimental analysis. Availability was assessed using a web search engine. Cost was calculated by finding the median prices of the ten most popular product variants found from United Kingdom (UK) suppliers. The remaining information was sourced from data sheets from the manufacturers listed.

Adhesive type	Major manufacturers	Readily available in the UK?	Adhesive price (GBP/100ml)	Shear strength (MPa)	Peel strength (N/mm)	Water resistance	Chemical resistance	Cure at room temperature?	Forms
Acrylics	Huntsman, Loctite, Permabond, 3M	Yes	34	14-24	2-9	Good	Good	Yes	Liquid, paste
Bismaleimides	Hexcel, Loctite	No	Not found	14-28	1-4	Good	Very good	No	Film
Cyanoacrylates	Bostik, Huntsman, Loctite, Permabond, 3M	Yes	91	7-14	1-4	Poor	Poor	Yes	Liquid
Epoxies	Huntsman, Loctite, Permabond, 3M	Yes	28	2-42	5-7	Good-excellent	Excellent	Yes	Liquid, paste
Methacrylates	Bostik, Huntsman, Permabond, Scott Bader, VuduGlu	Yes	17	20-40	6	Excellent	Excellent	Yes	Paste
Phenolics	3M	No	Not found	9	3	Good	Good	No	Film
Polyimides	Cytec	No	Not found	14-28	1	Excellent	Good	No	Film
Polyurethanes	Huntsman, Loctite, Permabond, 3M	Yes	16	7-17	6-7	Excellent	Excellent	Yes	Liquid, paste
Silicones	Loctite, Master Bond	Yes	6	1-7	1-7	Excellent	Good	Yes	Paste
Thermoplastics	Bostik, Loctite, 3M	No	3	1-2	1	Good	Average	Yes	Solid

Table 33: Comparison of adhesives considered for investigation

B Joining method selection tables

Tables 34-36 define design criteria that can be used to compare joining methods. Judgments of the performance of mechanical fastening and hybrid joining relative to adhesive bonding (the datum) are indicated. Also shown are weights reflecting the rationale of a track-side car maintenance team.

Stage	Consideration	Criterion	Description (* indicates that a lower value is preferred)	Adhesive bonding	Mechanical fastening	Hybrid joining	Weight
Design	Versatility	Combinations of materials	Ability to join dissimilar materials	–	0	0	0
		Joint geometries	Number of possible joint configurations	–	0	0	0
		Loading regimes	Suitability to a range of loading scenarios	–	1	0	0
	Effect on overall car design	Mass	Contribution to the overall mass of the car*	–	-1	-1	1
		Size	Space required in the design of the car*	–	-1	-1	1
Analysis	Predictability	Knowledge base	Availability of information	–	1	0	0
		Accuracy of theoretical models	Agreement between predictions and results	–	1	-1	0
		Ease of testing	Simplicity of specimen manufacture and testing	–	1	-1	0
Procurement	Availability	Lead time	Time from ordering to delivery*	–	0	0	0
		Reliability of supply	Number of possible suppliers	–	1	-1	0
	Cost	Adhesive/fastener	Cost of adhesive/fastener per joint*	–	0	-1	0
		Labour	Time for which a manual worker is required*	–	1	-1	0
		Waste material	Cost of excess material not used in joining*	–	1	0	0
		Tooling/equipment	Cost of tooling/equipment required for joining*	–	-1	-1	1

Table 34: Design criteria for joining methods (part 1 of 3)

Stage	**Consideration**	**Criterion**	**Description (* indicates that a lower value is preferred)**	**Adhesive bonding**	**Mechanical fastening**	**Hybrid joining**	**Weight**
Manufacture and assembly	Processability	Ease of manufacture and assembly	Number of processes to complete and parts to handle*	–	-1	-1	1
		Joining time	Time taken to produce a working joint*	–	1	0	1
		Processing environment	Sensitivity of joint quality to processing conditions*	–	1	0	1
		Skill level	Sensitivity of joint quality to worker expertise*	–	1	0	1
		Health and safety	Number of precautions required*	–	-1	-1	1
Operation	Loading performance	Tension	Stiffness and strength in tension	–	1	0	1
		Compression	Stiffness and strength in compression	–	0	0	1
		Shear	Stiffness and strength in shear	–	-1	-1	1
		Bending	Stiffness and strength in bending	–	1	-1	1
		Torsion	Stiffness and strength in torsion	–	1	0	1
		Impact	Impact strength	–	1	0	1
		Fatigue	Fatigue strength at ten million cycles	–	-1	-1	1

Table 35: Design criteria for joining methods (part 2 of 3)

Stage	Consideration	Criterion	Description (* indicates that a lower value is preferred)	Adhesive bonding	Mechanical fastening	Hybrid joining	Weight
Operation	Environmental degradation	Mechanical wear	Susceptibility to wear due to solid friction	–	-1	-1	0
		Temperature	Sensitivity of performance to operating temperature*	–	1	0	1
		Moisture	Sensitivity of performance to moisture levels*	–	1	0	1
		Chemicals	Sensitivity of performance to chemical exposure*	–	1	0	1
		Radiation	Sensitivity of performance to radiation exposure*	–	1	0	1
	Maintenance	Ease of inspection	Ability to assess joint condition	–	1	0	1
		Ease of disassembly	Ability to separate joint components	–	1	1	1
		Ease of repair	Ability to return to working order without full replacement	–	1	0	1
End of life		Ease of re-use/recycling	Ability to repurpose for joining or recover unwanted material	–	1	0	0
		Ease of disposal	Simplicity of disposing of unwanted material	–	1	0	0

Table 36: Design criteria for joining methods (part 3 of 3)